ABDUS SALAM INTERNATIONAL CENTRE FOR THEORETICAL PHYSICS

Physics and Dynamics of the Ocean

Riccardo Farneti

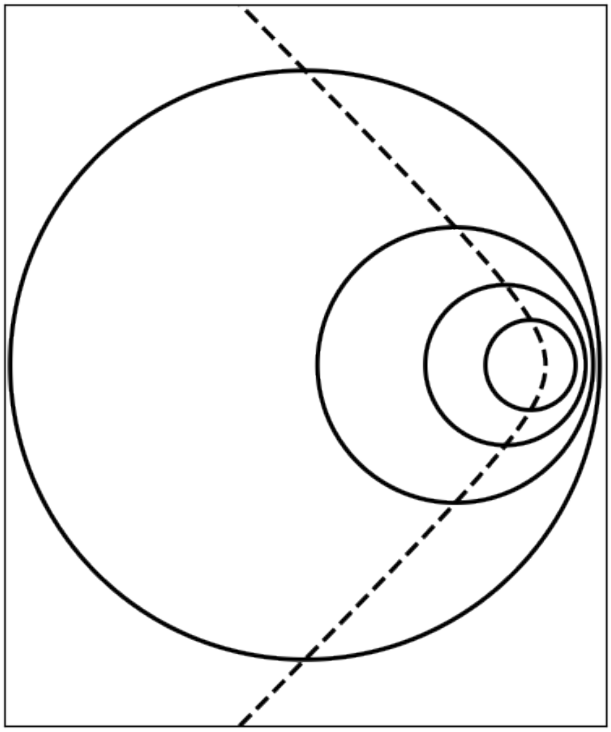

EARTH SYSTEM PHYSICS DIPLOMA PROGRAMME
2022-2023

Preface

These notes form the basis for the *Physics and Dynamics of the Ocean* Course of the Abdus Salam International Centre for Theoretical Physics Diploma Programme in Earth System Physics.

Some of the material on these notes is *borrowed* from *Vallis* (2006); *Talley et al.* (2011); *Olbers et al.* (2012); *Vallis* (2019). Students are encouraged to supplement these notes with readings of those and more textbooks.

The notes will grow in time, and comments and suggestions are highly appreciated.

This is the version from April 14, 2023.

Riccardo Farneti
(rfarneti@ictp.it)

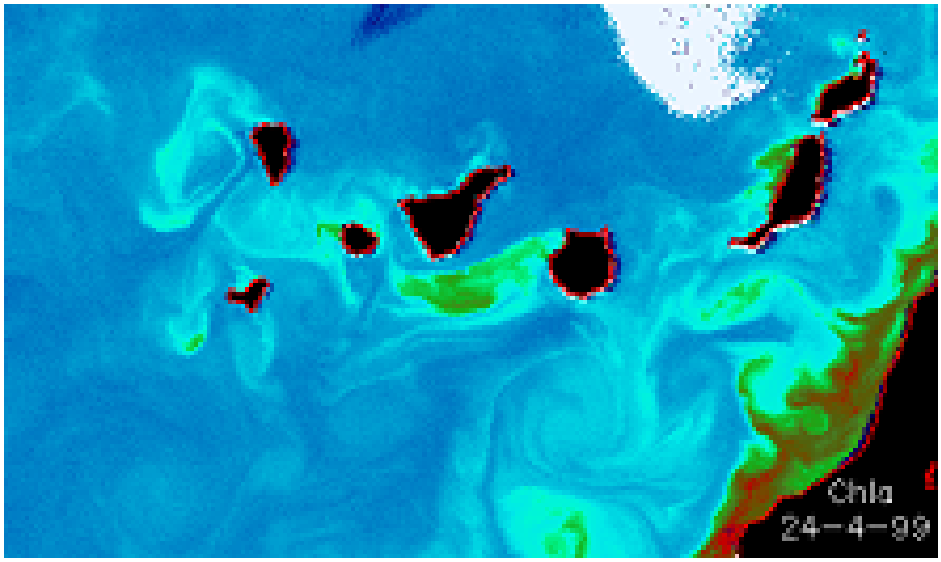

Satellite image from SeaWIFS showing surface Chl-a concentration on the north-west coast of Africa around the Canary Islands. Notice the downstream cyclonic and anticyclonic eddies formed by the interaction of the Canary Current with the islands and the coastal upwelling shedding filaments and eddies.

List of Figures

1 Satellite image from SeaWIFS showing surface Chl-a concentration on the north-west coast of Africa around the Canary Islands. Notice the downstream cyclonic and anticyclonic eddies formed by the interaction of the Canary Current with the islands and the coastal upwelling shedding filaments and eddies. 3

1.1 Net heat and freshwater fluxes computed from the NCEP/NCAR reanalysis for the period 2010-2019 *Kalnay et al.* (1996). 12

1.2 Surface zonal and meridional components of the wind stress computed from the NCEP/NCAR reanalysis for the period 2010-2019 *Kalnay et al.* (1996). 12

1.3 Zonal-mean of the climatological (2005-2012) Temperature and Salinity for the Atlantic Ocean at 30W and Pacific Ocean at 170W from in situ profile data (World Ocean Atlas 2013 version 2) at 0.25 degree horizontal resolution. 13

1.4 A schema of the main currents of the global ocean [from *Vallis* (2006)]. 14

1.5 Climatological mean (2005-2012) Sea Surface Temperature and Sea Surface Salinity for the global ocean from in situ profile data (World Ocean Atlas 2013 version 2) at 0.25 degree horizontal resolution. 15

1.6 A schema of the stratification and overturning circulation. [from *Vallis* (2006)] 16

1.7 A schema of the thermohaline circulation (THC), or the Meridional Overturning Circulation (MOC). [from *Kuhlbrodt et al.* (2007)] 16

1.8 The global MOC as computed from a Coupled General Circulation Model (CGCM). We clearly see the presence of the North Atlantic Deep Water cell, the interhemispheric meridional circulation, a locally-circulating deacon Cell, and two SubTropical Cells. Each meridional cell is driven by different dynamics and all together set up the global ocean circulation. 17

2.1 *Climatological mean (2005-2012) Sea Surface Temperature and Sea Surface Salinity for the global ocean from in situ profile data (World Ocean Atlas 2013 version 2) at 0.25 degree horizontal resolution.* 20
2.2 *Zonal-mean of the climatological (2005-2012) Temperature and Salinity for the Atlantic Ocean at 30W and Pacific Ocean at 170W from in situ profile data (World Ocean Atlas 2013 version 2) at 0.25 degree horizontal resolution.* 21

3.1 *Coordinate frame (x_1, x_2, x_3) rotating at angular velocity Ω with respect to a fixed frame (X_1, X_2, X_3).* 28
3.2 *Components of the angular velocity vector for a point on the sphere.* 31
3.3 *A cartesian reference system (x,y,z) and its associated spherical system (r, θ, ϕ) around the point (a, θ_0, ϕ_0). The plane $z = 0$ (or β-plane) is tangent to the sphere around the point (a, θ_0, ϕ_0). The approximation $tan(\theta - \theta_0) \approx (\theta - \theta_0)$ is well justified for small variations in latitude. On the β-plane, the rotation vector is $\boldsymbol{k}\Omega\, sin\theta$, where $sin\theta \approx sin\theta_0 + (y/a)cos\theta_0$.* 32
3.4 *The Coriolis parameter f and its meridional gradient β as a function of latitude.* 33
3.5 Schematic of a geostrophically balanced flow with a positive value of the Coriolis parameter f. Flow is parallel to the lines of constant pressure. Cyclonic flow is anticlockwise around a low pressure region. [from *Vallis* (2006)] . . . 37
3.6 Schematic of thermal wind balance in the northern hemisphere. Shown are surfaces of constant density, or isopycnals. Density increases with depth and latitude, $\rho_3 > \rho_2 > \rho_1$. The termal wind associated with this density field is eastward, or out of the page, and decreases with depth. The same eastward thermal wind velocity would have resulted in the southern hemisphere, with $\rho_y < 0$ and $f < 0$. 39
3.7 A global map of the first baroclinic gravity wave phase speed and its zonal mean. [data from Chelton et al., 1998] 42

3.8 A global map of the first baroclinic Rossby radius of deformation and its zonal mean. [data from Chelton et al., 1998] . 43

3.9 The oceanic resolution needed to resolve the Rossby Radius of deformation in an ocean model [from Hallberg et al., 2013]. 44

3.10 The same ocean model at different horizontal resolutions, increasing from right to left. 44

3.11 Schematic of a flat-bottomed shallow-water system and mass balance within a column of fluid. 47

3.12 Zonal-mean potential density in the latitudes of the Drake Passage. 48

4.1 *Dispersion relation for Poincarè and Kelvin waves. The frequency is scaled by f and the wavenumber by L_d. The black dot marks the inertial oscillations regime and the $\omega = 0$ is the geostrophic case.* 51

4.2 *For a system bounded to the west (x positive) the wave propagates in the negative y direction, i.e. to the south. If x is negative this reverses so on the eastern side of the basin the Kelvin wave propagates northwards. In the northern hemisphere a Kelvin wave will keep the coast to its right as it pushed against it by the Coriolis force.* 53

4.3 *Rossby wave dispersion relation, phase and group speeds.* 58

4.4 *Rossby wave dispersion diagram. Contours are of frequency in units of $\beta\, L_d$. The group velocity, the gradient of the frequency in wavenumber space, is normal to the contours and inversely proportional to the spacing between contours. The hyperbola separating waves with eastward and westward group velocity is shown by the dashed line and is $\kappa^2 = l^2 + L_d^{-2}$. Frequency contours reduce to a single point when $\omega = 0.5\beta L_d$ and $\kappa = L_d$.* 59

4.5 Upper panel: the dispersion relation for the barotropic and first two baroclinic modes of the 3-layer QG ocean. Shown are values of both positive and negative wavenumbers. The wavenumber is scaled by the deformation radius L_d and the frequency by βL_d; the meridional wavenumber l is set to zero. The first baroclinic mode frequency reaches a maximum at $\omega_{max} = \beta L_d/2$, i.e. $\omega_{max} = |0.5|$. Lower panel: phase (solid lines, $c_x = \omega/k$) and group (dashed lines, $Cg_x = \partial\omega/\partial k$) velocities of the barotropic and first two baroclinic modes, scaled by βL_d^2. 62

4.6 Sea surface height anomalies showing the propagation of planetary waves in the Pacific Ocean. Also clear is the β-effect inducing larger phase speeds towards the equator [from *Chelton and Schlax* (1996)]. 64
4.7 Time-longitude plot of the sea surface height anomalies (in meters) in the Indian Ocean at 20^oS. On the left panels, the original altimeter data. On the right panel, the corresponding westward-filtered signature. There is a clear evidence of crests and troughs propagating westward with a biannual period (Courtesy of P. Cipollini). 65
4.8 *A global contour map of the baroclinic gravity wave phase speed [from Chelton et al., 1998] and its zonal mean.* 67
4.9 *As in Fig.4.8 but from the GFDL-CM4.0 model under historical conditions for years 2010-2014.* 68
4.10 *A global contour map of the baroclinic Rossby radius of deformation and its zonal mean. [data from Chelton et al., 1998]* 70
4.11 *As in Fig.4.10 but from the GFDL-CM4.0 model under historical conditions for years 2010-2014.* 71
4.12 *A global contour map of the baroclinic Rossby wave phase speed and its zonal mean. [data from Chelton et al., 1998]* 72
4.13 *As in Fig.4.12 but from the GFDL-CM4.0 model under historical conditions for years 2010-2014.* 73
4.14 *Surface layer thickness after a thermohaline overturning of 10 Sv is switched on at time t = 0 in the northwest corner of an ocean initially at rest. There is no wind forcing, and the surface layer is initially 500 m deep. The contour interval is 2 m, and thicknesses less than 499 m are shaded. Note that the thickness anomaly on the western boundary is much greater than that in the interior. [from Johnson and Marshall, JPO2022]* 75
4.15 *The baroclinic gravity wave phase speed computed from the GFDL-CM4.0 model under historical conditions for years 2010-2014.* . . 77
4.16 *The baroclinic gravity wave phase speed computed from the GFDL-CM4.0 model for the future scenario SSP585.* 78
4.17 *The Rossby radius computed from the GFDL-CM4.0 model under historical conditions for years 2010-2014.* 79
4.18 *The Rossby radius computed from the GFDL-CM4.0 model for the future scenario SSP585.* 80
4.19 *The baroclinic Rossby wave phase speed computed from the GFDL-CM4.0 model under historical conditions for years 2010-2014.* . . 81
4.20 *The baroclinic Rossby wave phase speed computed from the GFDL-CM4.0 model for the future scenario SSP585.* 82

Contents

1 Introduction **11**

2 Thermodynamics of Seawater **19**
2.1 Thermodynamics of seawater 19
2.2 Temperature, Salinity, Density and Stratification 19
2.2.1 Buoyancy frequency 19

3 Fundamental tools **23**
3.1 Kinematics 23
3.1.1 Lagrangian Derivative 24
3.1.2 Streamlines and streamfunctions 24
3.1.3 (Gauss') Divergence theorem 25
3.1.4 Stokes' theorem 26
3.2 The equations of motion 27
3.2.1 Motion in a rotating frame of reference 28
3.2.2 Thin shell approximation 30
3.2.3 The β-plane 31
3.3 Kinematical and dynamical approximations 34
3.3.1 Hydrostatic balance 34
3.3.2 Hydrostatic approximation 36
3.3.3 Shallow water approximation 36
3.3.4 Boussinesq approximation 36
3.3.5 Rigid lid approximation 36
3.4 Rossby number 36
3.5 Geostrophic and Thermal Wind Balance 36
3.6 The Rossby radius 40
3.7 The shallow-water equations 46

4 Waves in the ocean **49**
4.1 Poincaré Waves 49
4.2 Kelvin Waves 52
4.3 Planetary, or Rossby, waves 55
4.3.1 Quasi-geostrophic Rossby waves 60
4.3.2 Rossby waves in observations and models 64

Chapter 1

Introduction

We shall discuss the basic principles and dynamics setting up the large-scale ocean circulation. We will make use of all concepts we have developed in our previous courses (Geophysical Fluid Dynamics, Physics of the Ocean) and we will probably see some topics that have been mentioned in other courses (e.g., Atmospheric dynamics). But, *repetita iuvant!*. And those same principles will be applied here to ocean dynamics, perhaps in a revised way.

The large-scale ocean circulation can be broadly divided into two different kinds, a *horizontal surface wind-driven circulation* and a *meridional deep buoyancy- and wind-driven circulation*, although the distinction is only a bad approximation as they are intimately connected. This is particularly so for the meridional overturning which is driven both by buoyancy and wind at the surface.

Ocean circulation theory is based on the very same principles that drive atmospheric circulation, and many theories have been borrowed from the meteorological and atmospheric fields. Of course, the ocean is just another geophysical fluid, and as such it is governed by all GFD conservation principles, forces and instabilities you have been exposed already. There are two main differences with respect to the atmosphere that are worth pointing out now.

- First, contrary to the atmosphere, the ocean is heated and cooled from above (Fig. 1.1).

- Second, ocean circulation is often constrained by the presence of continents, and this will alter the structure and dynamics of the flow (Fig. 2.2).

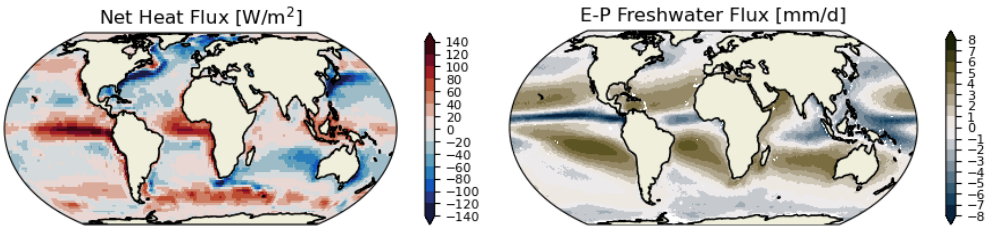

Figure 1.1: Net heat and freshwater fluxes computed from the NCEP/NCAR reanalysis for the period 2010-2019 *Kalnay et al.* (1996).

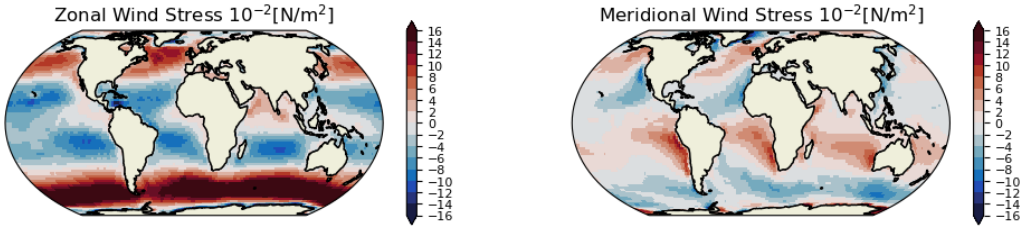

Figure 1.2: Surface zonal and meridional components of the wind stress computed from the NCEP/NCAR reanalysis for the period 2010-2019 *Kalnay et al.* (1996).

These two peculiarities will explain some of the differences between oceanic and atmospheric circulation, as well as some geographical uniqueness in ocean circulation.

The ocean is largely driven by surface wind stress (Fig. 1.2) –actually not the stress but its curl! ... see later–, and common patterns arise in the surface wind-driven large-scale circulation of all different basins (Fig. 1.4). They all have just a few common ingredients, and these will qualitatively explain the main features of the wind-driven gyres. The Southern Ocean is a rather different story, and it will be discussed separately.

However, buoyancy forcing –the sum of surface heat and freshwater fluxes (Fig. 1.1)– and the latitudinal extent of the ocean basins, will alter the way the surface of each basin is buoyancy forced, with profound implications for the interior temperature and salinity structure as well as deep circulations of the oceans (Fig. 2.2, Fig. 2.1). Once we have highlighted the major circulations and their relations, a clear picture of the interior and meridional circulation will also appear.

There is a good observational and theoretical understanding of the major processes responsible for the Meridional Overturning Circulation (MOC) (Fig. 1.6). This is not the same in each and every basin (Fig. 1.7),

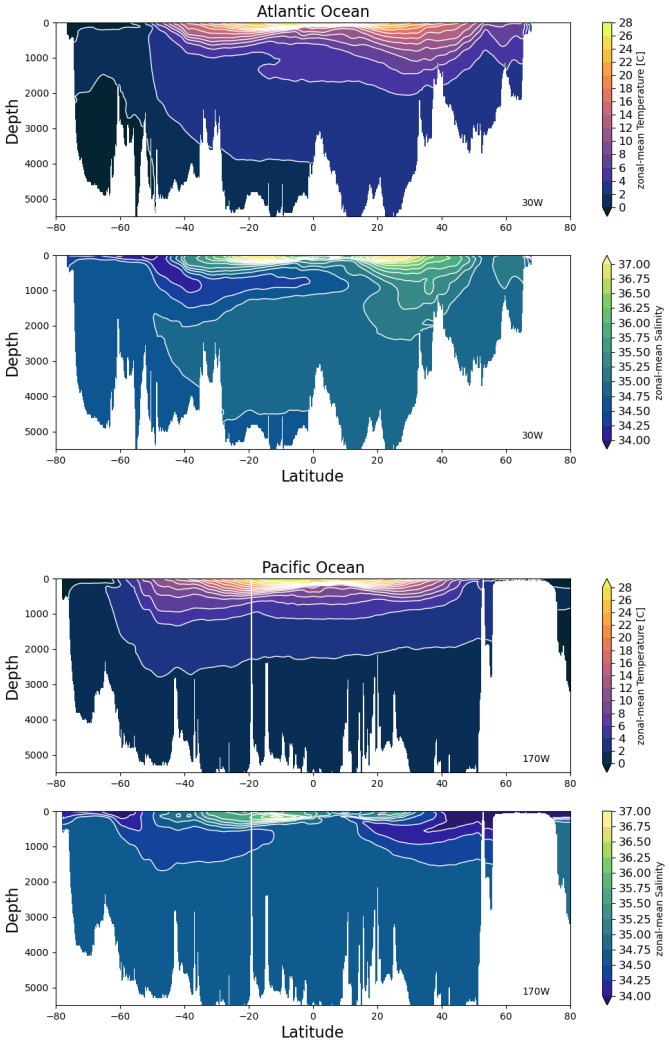

Figure 1.3: Zonal-mean of the climatological (2005-2012) Temperature and Salinity for the Atlantic Ocean at 30W and Pacific Ocean at 170W from in situ profile data (World Ocean Atlas 2013 version 2) at 0.25 degree horizontal resolution.

and fundamental differences exist giving rise to shallow and deep circulations, responsible for different degrees of meridional energy and mass transports. Our present models capture these features reasonably well (Fig. 1.8), although many small-scale effects are missing or poorly parameterized, and most importantly the variability of this circulation is not well understood (let alone its future evolution!).

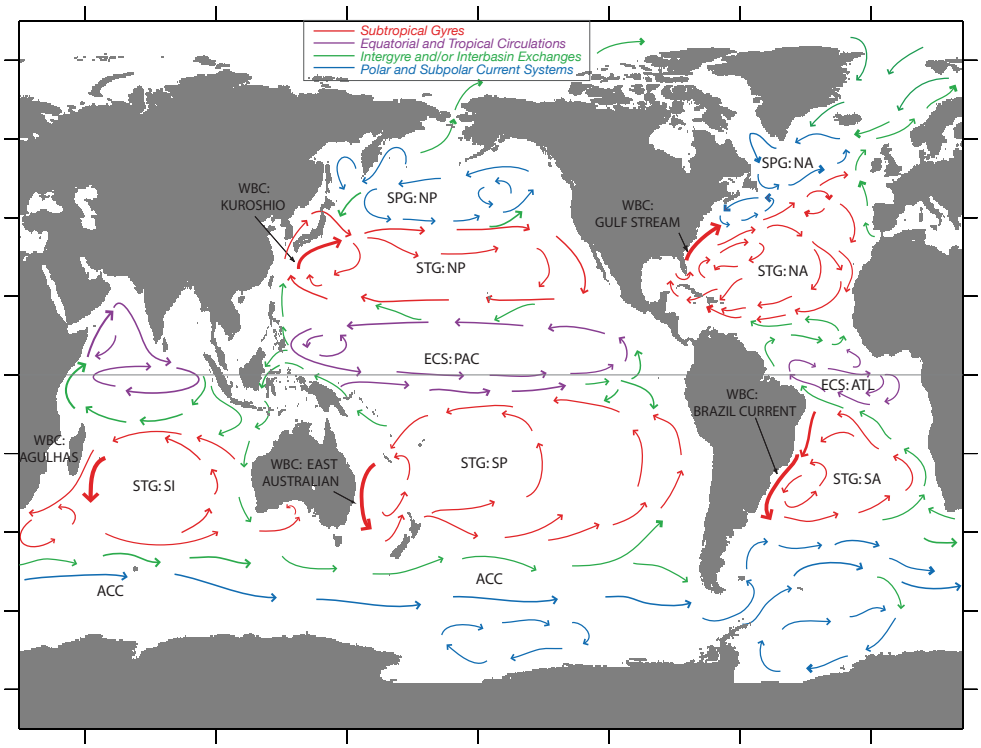

Figure 1.4: A schema of the main currents of the global ocean [from *Vallis* (2006)].

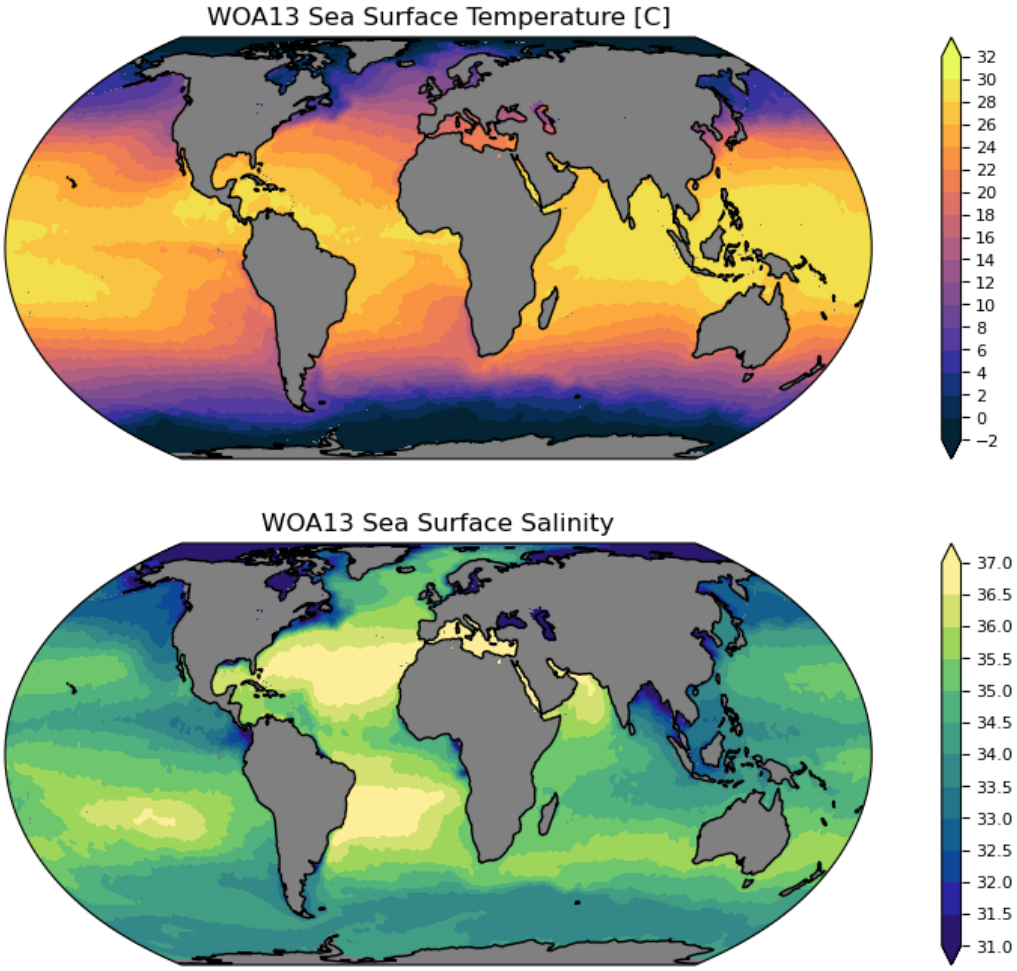

Figure 1.5: Climatological mean (2005-2012) Sea Surface Temperature and Sea Surface Salinity for the global ocean from in situ profile data (World Ocean Atlas 2013 version 2) at 0.25 degree horizontal resolution.

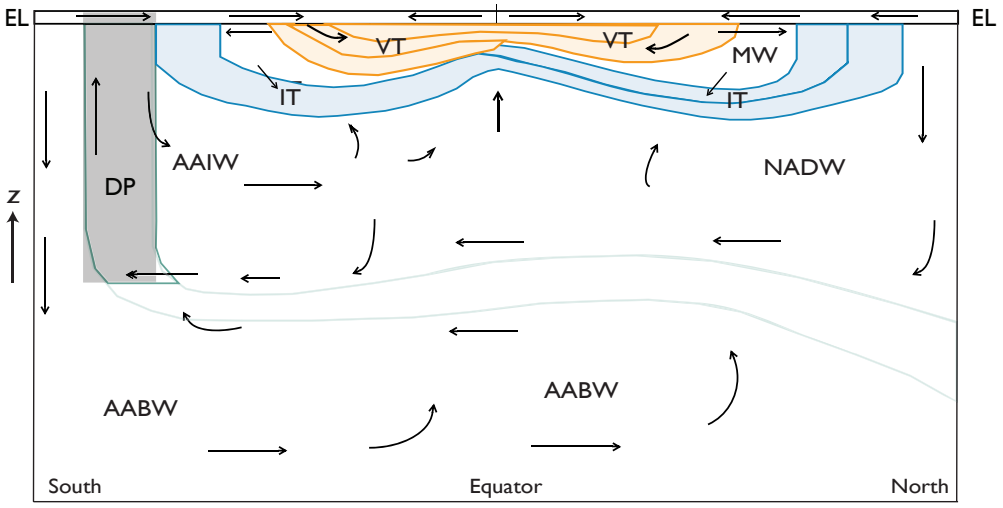

Figure 1.6: A schema of the stratification and overturning circulation. [from *Vallis* (2006)]

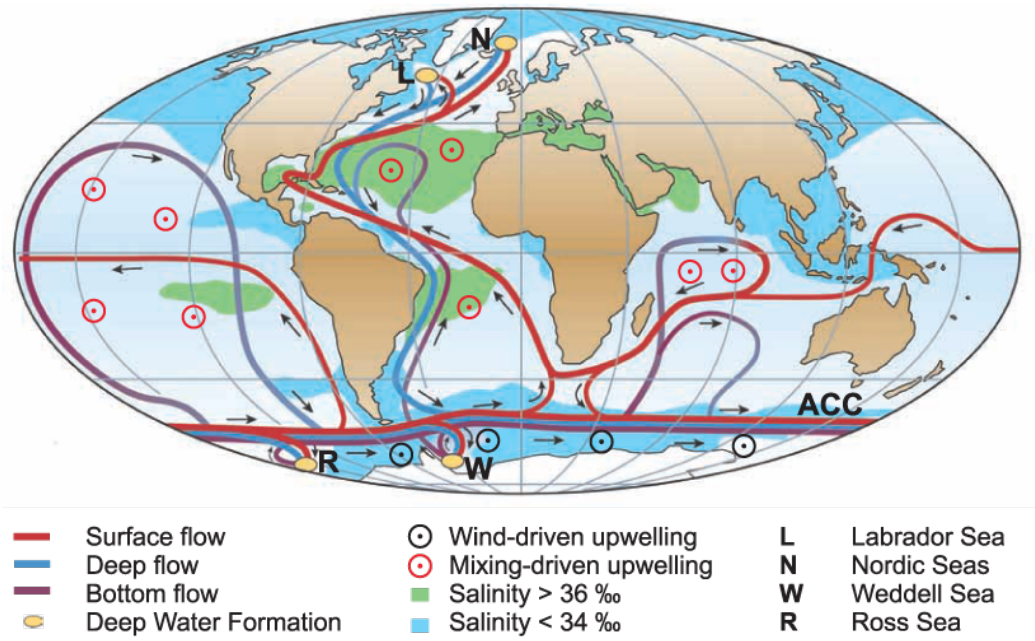

Figure 1.7: A schema of the thermohaline circulation (THC), or the Meridional Overturning Circulation (MOC). [from *Kuhlbrodt et al.* (2007)]

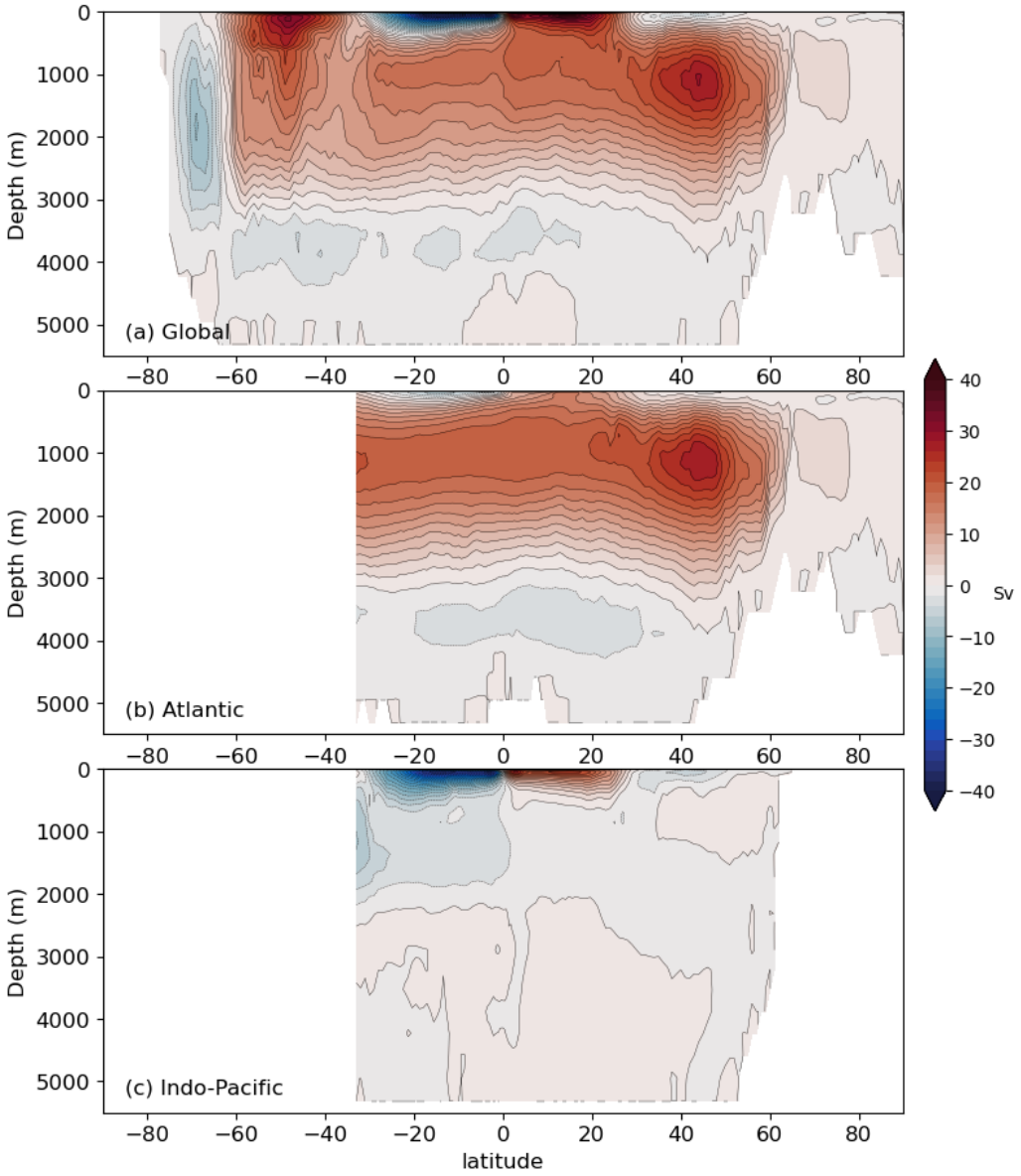

Figure 1.8: The global MOC as computed from a Coupled General Circulation Model (CGCM). We clearly see the presence of the North Atlantic Deep Water cell, the interhemispheric meridional circulation, a locally-circulating deacon Cell, and two SubTropical Cells. Each meridional cell is driven by different dynamics and all together set up the global ocean circulation.

Chapter 2

Thermodynamics of Seawater

2.1 Thermodynamics of seawater

2.2 Temperature, Salinity, Density and Stratification

2.2.1 Buoyancy frequency

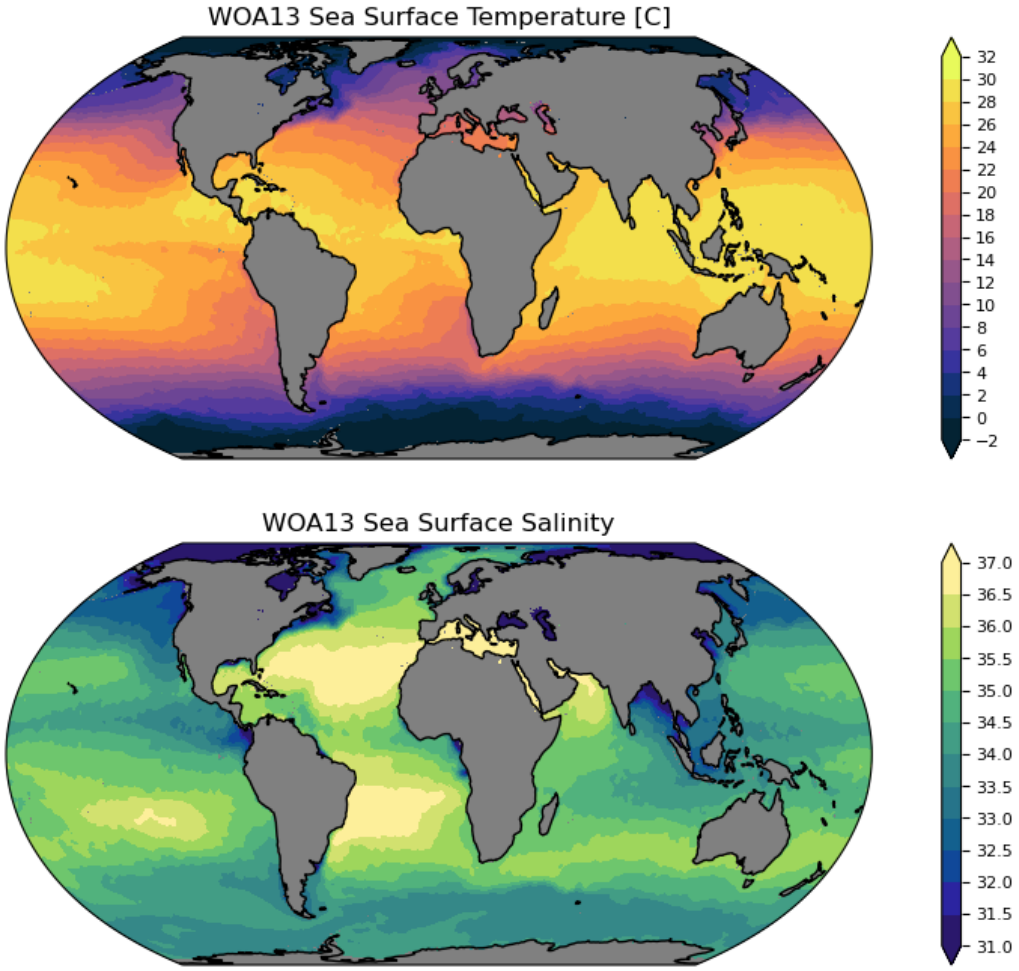

Figure 2.1: *Climatological mean (2005-2012) Sea Surface Temperature and Sea Surface Salinity for the global ocean from in situ profile data (World Ocean Atlas 2013 version 2) at 0.25 degree horizontal resolution.*

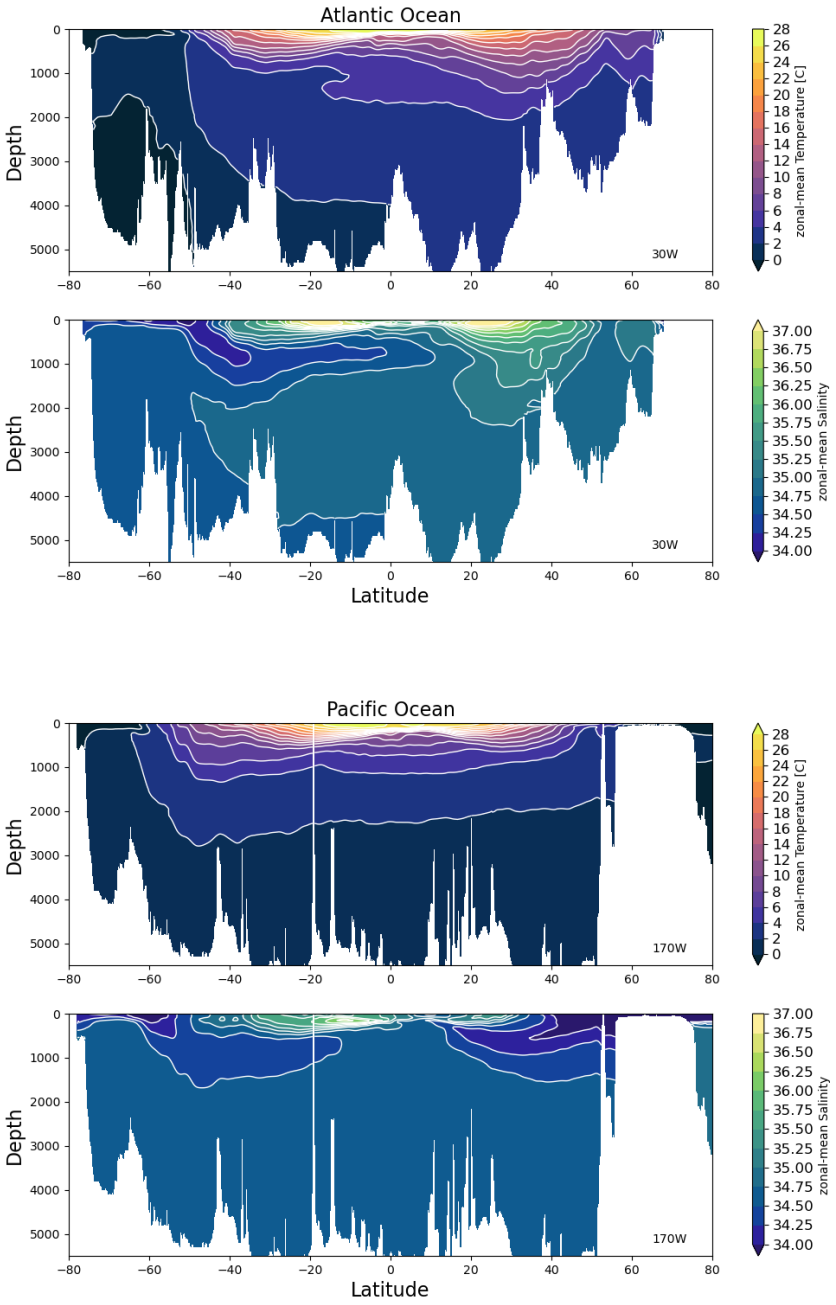

Figure 2.2: *Zonal-mean of the climatological (2005-2012) Temperature and Salinity for the Atlantic Ocean at 30W and Pacific Ocean at 170W from in situ profile data (World Ocean Atlas 2013 version 2) at 0.25 degree horizontal resolution.*

Chapter 3

Fundamental tools

We have already discussed the Geostrophic equations, or *g*eostrophic balance, in previous courses (*Geophysical Fluid Dynamics*, and maybe in Atmospheric Dynamics too!), but it is good to restate our assumptions and starting point (*repetita iuvant!*).

3.1 Kinematics

- In the LAGRANGIAN description of motion, one essentially follows the history of an individual particle. A flow variable $F(r_0, t)$ and its velocity is given by $u_i = \mathrm{d}(r_i)/\mathrm{d}t$
- In the EULERIAN description one focuses on what happens at a spatial point r, so the flow variable is $F(r, t)$.
- In the Eulerian case, $\mathrm{d}/\mathrm{d}t$ gives the local rate of change of F at each point r and is not the total rate of change seen by a fluid particle ...

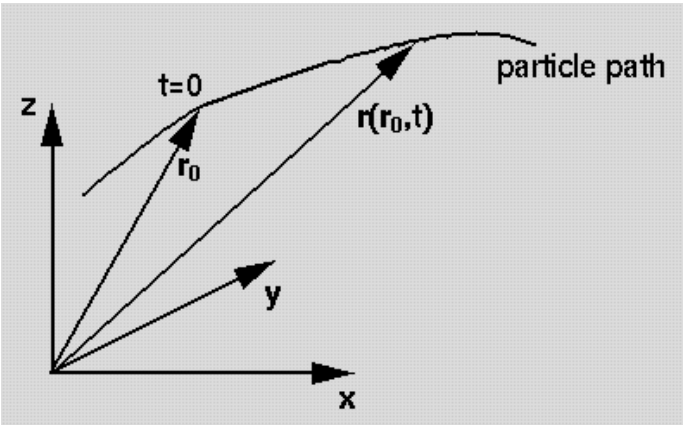

3.1.1 Lagrangian Derivative

We seek to calculate the rate of change of F at each point following a particle of fixed identity.

$$\boxed{\frac{DF}{Dt} = \frac{\partial F}{\partial t} + u_i \frac{\partial F}{\partial x_i}} \tag{3.1}$$

The Lagrangian Derivative $\frac{DF}{Dt}$ is made of (1) the local rate of change at a given point (zero for steady flows...) and (2) the advective derivative.

$\frac{\partial F}{\partial t}$ is the local rate of change of F at a given point.

$u_i \frac{\partial F}{\partial x_i}$ is the advective derivative, it is the change in F as a result of advection of the particle from one location to another where F is different.

3.1.2 Streamlines and streamfunctions

The streamline

- At $t = t_0$, streamlines are curves that are tangent to direction of flow.
- For unsteady flows, streamlines change with time.

Let $ds = (dx, dy, dz)$ be an element of arc length along a streamline, and let $u = (u, v, w)$ be the local velocity vector along that streamline, then $dx/u = dy/v = dz/w$.

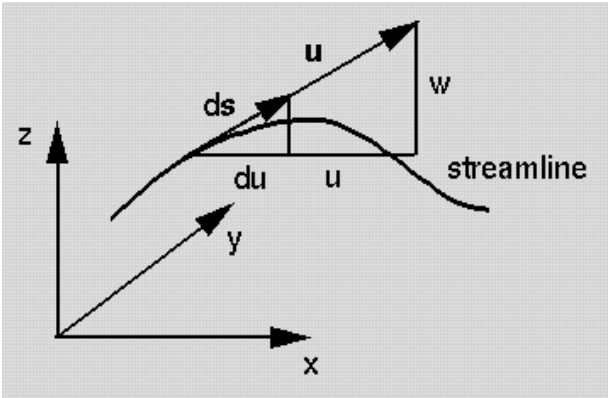

- Close to a solid boundary, streamlines are parallel to that boundary.
- The direction of the streamline is the direction of the fluid velocity.
- Fluid can not cross a streamline.

- Streamlines can not cross each other.
- Any particle starting on one streamline will stay on that same streamline.
- In unsteady flow, streamlines can change position with time.
- **Streamlines** are a family of curves that are instantaneously tangent to the velocity vector of the flow. These show the direction a fluid element will travel in at any point in time.
- **Pathlines** are the trajectories that individual fluid particles follow. These can be thought of as a ″recording″ of the path a fluid element in the flow takes over a certain period. The direction the path takes will be determined by the streamlines of the fluid at each moment in time.
- For a steady flow, the two are the same.

The streamfunction

3.1.3 (Gauss') Divergence theorem

The theorem relates a volume integral to a surface integral. Consider a volume V bounded by a closed surface A. Consider an infinitesimal surface element dA whose outward unit normal is **n**. The vector ndA has magnitude dA and direction **n**.

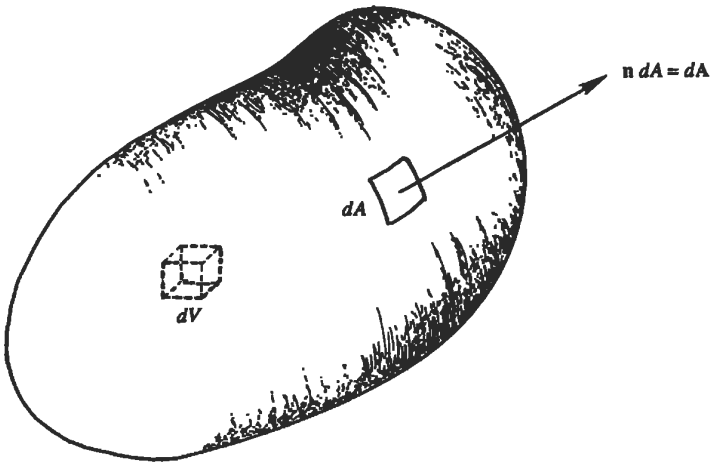

Gauss' theorem states that the volume integral of the divergence of **Q** is equal to the surface integral of the outflow of **Q**.

$$\int_v \frac{\partial Q}{\partial x_i} \mathrm{d}V = \int_A \mathrm{d}A_i Q \tag{3.2}$$

For a vector $\boldsymbol{Q}$:

$$\boxed{\int_v \frac{\partial Q_i}{\partial x_i} \mathrm{d}V = \int_A \mathrm{d}A_i Q}, \tag{3.3}$$

which is now called the Divergence Theorem. In vector notation

$$\int_v \nabla \cdot \mathbf{Q} \, \mathrm{d}V = \int_A \mathrm{d}\mathbf{A} \cdot \mathbf{Q} \tag{3.4}$$

3.1.4 Stokes' theorem

The theorem relates a surface over an open surface to a line integral. Consider an open surface A, with bounding curve C. Let $d\mathbf{r}$ be an element of the bounding curve whose direction is that of the tangent.

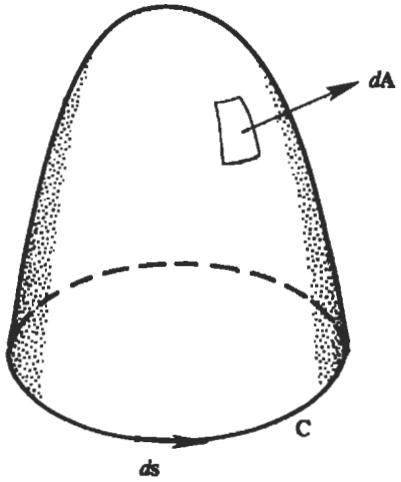

Stokes' theorem states that

$$\boxed{\int_A (\nabla \times \mathbf{F}) \cdot \mathrm{d}\mathbf{A} = \int_C \mathbf{F} \cdot \mathrm{d}\mathbf{r}} \tag{3.5}$$

the surface integral of the curl of a vector field **F** is equal to the line integral of **F** along the bounding curve. The line integral of a vector around a closed curve C is the *circulation of the field about C*.

Prove that $div(curl\, \boldsymbol{u}) = 0$, for any vector $\boldsymbol{u}$.

3.2 The equations of motion

There can be two kind of forces acting on fluids. Body forces, and we will restrict our attention, for now, to gravitational force per unit mass

$$\mathbf{g} = -\nabla(gz) = -\hat{k}\frac{\partial(gz)}{\partial z} = -\hat{k}g \tag{3.6}$$

and surface forces, which can be normal or tangential to the fluid. Normal forces will be relate to pressure, whereas tangential forces will be related to shear stresses.

In order to derive a principle of conservation of momentum we will start by applying Newton's law of motion to an infinitesimal element of fluid. The continuity equation, for an element of fluid of constant density is

$$\frac{\partial \rho}{\partial t} + \nabla \cdot (\rho \mathbf{u}) = 0 \tag{3.7}$$

and we multiply this by $\mathbf{u}$:

$$\frac{\partial(\rho u)}{\partial t} + \frac{\partial(\rho u^2)}{\partial x} + \frac{\partial(\rho uv)}{\partial y} + \frac{\partial(\rho uw)}{\partial z} = f_x \tag{3.8}$$

$$\frac{\partial(\rho v)}{\partial t} + \frac{\partial(\rho vu)}{\partial x} + \frac{\partial(\rho v^2)}{\partial y} + \frac{\partial(\rho vw)}{\partial z} = f_y \tag{3.9}$$

$$\frac{\partial(\rho w)}{\partial t} + \frac{\partial(\rho wu)}{\partial x} + \frac{\partial(\rho wv)}{\partial y} + \frac{\partial(\rho w^2)}{\partial z} = f_z \tag{3.10}$$

$$\tag{3.11}$$

which for a constant density reduces to

$$\rho\left(\frac{\partial}{\partial t} + \mathbf{u}\cdot\nabla\right)\mathbf{u} = \mathbf{f} \tag{3.12}$$

If we express our body force per unit volume $\rho\mathbf{g}$, we arrive to the Cauchy equation of motion

$$\rho\frac{\mathrm{D}\,u_i}{\mathrm{D}\,t} = \rho g_i + \frac{\partial \tau_{ij}}{\partial x_j} \tag{3.13}$$

where the stress tensor τ_{ij} includes all surface forces. Using the constitutive equation for a Newtonian fluid, we now arrive to the Navier-Stokes equation

$$\rho\frac{\mathrm{D}\,u_i}{\mathrm{D}\,t} = \rho\mathbf{g} - \nabla p + \mu\nabla^2\mathbf{u} \tag{3.14}$$

which reduces to the Euler equation under the assumption of frictionless flow

$$\rho \frac{\mathrm{D}\, u_i}{\mathrm{D}\, t} = \rho \mathbf{g} - \nabla p \tag{3.15}$$

3.2.1 Motion in a rotating frame of reference

Eq.3.28 is valid for an inertial or fixed frame of reference. But in GFD we measure positions and velocities relative to a frame of reference fixed on the surface of the Earth, which rotates w.r.t. to a frame inertial.

Let's have a frame of reference (x_1, x_2, x_3) rotating at a uniform angular velocity $\mathbf{\Omega}$ w.r.t. a fixed frame (X_1, X_2, X_3). Any vector $\mathbf{P}$ is represented by

$$\mathbf{P} = P_1 i_1 + P_2 i_2 + P_3 i_3 \tag{3.16}$$

For a fixed observer, the directions of the rotating unit vectors (i_1, i_2, i_3) change with time. The time derivatives of $\mathbf{P}$ is thus

$$\begin{aligned} \left(\frac{d\mathbf{P}}{dt}\right)_F =& \frac{d}{dt}(P_1 i_1 + P_2 i_2 + P_3 i_3) = \\ & i_1 \frac{dP1}{dt} + i_2 \frac{dP2}{dt} + i_3 \frac{dP3}{dt} + P_1 \frac{di_1}{dt} + P_2 \frac{di_2}{dt} + P_3 \frac{di_3}{dt} \end{aligned} \tag{3.17}$$

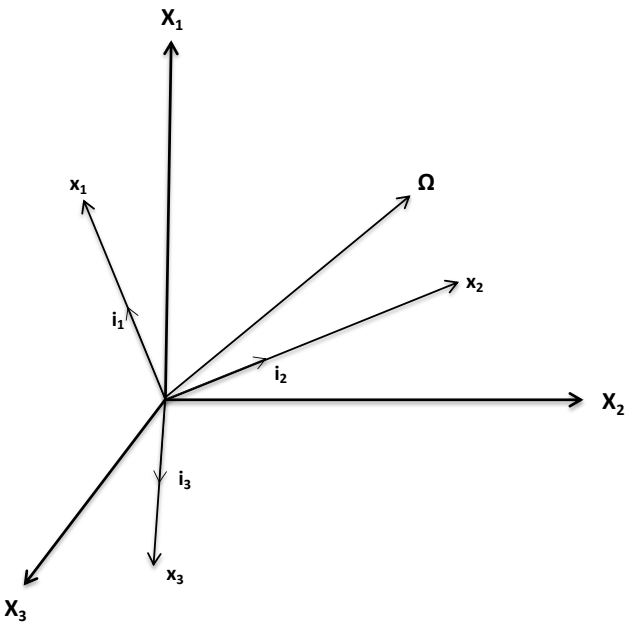

Figure 3.1: *Coordinate frame (x_1, x_2, x_3) rotating at angular velocity Ω with respect to a fixed frame (X_1, X_2, X_3).*

For an observer rotating with (x_1, x_2, x_3) the rate of change of $\mathbf{P}$ is equal to the first three terms in Eq.3.17, and so

$$\left(\frac{d\mathbf{P}}{dt}\right)_F = \left(\frac{d\mathbf{P}}{dt}\right)_R + P_1\frac{di_1}{dt} + P_2\frac{di_2}{dt} + P_3\frac{di_3}{dt} \tag{3.18}$$

Each unit vector i traces a cone with radius $\sin\alpha$, where α is a constant angle. i changes in time $\mathrm{d}t$ as $\mathrm{d}i = \sin\alpha d\theta$ which is the length travelled by the top of i. The rate fo change is thus

$$\frac{di}{dt} = \sin\alpha\left(\frac{d\theta}{dt}\right) = \sin\alpha\Omega \tag{3.19}$$

The direction of the rate of change is thus perpendicular to the plane $(\Omega, \mathbf{i})$, hence

$$\frac{d\mathbf{i}}{dt} = \mathbf{\Omega}\times\mathbf{i} \tag{3.20}$$

for any rotating vector $\mathbf{i}$, giving us

$$\left(\frac{d\mathbf{P}}{dt}\right)_F = \left(\frac{d\mathbf{P}}{dt}\right)_R + \mathbf{P}\times\mathbf{\Omega} \tag{3.21}$$

Applying this rule to the position vector $\mathbf{r}$

$$\left(\frac{d\mathbf{r}}{dt}\right)_F = \left(\frac{d\mathbf{r}}{dt}\right)_R + \mathbf{r}\times\mathbf{\Omega} \tag{3.22}$$

or

$$\mathbf{u}_F = \mathbf{u}_R + \mathbf{r}\times\mathbf{\Omega} \tag{3.23}$$

Applying this rule to the velocities

$$\left(\frac{d\mathbf{u_F}}{dt}\right)_F = \left(\frac{d\mathbf{u_F}}{dt}\right)_R + \mathbf{u_F}\times\mathbf{\Omega} \tag{3.24}$$

$$\left(\frac{d\mathbf{u_F}}{dt}\right)_F = \frac{d}{dt}\left(\mathbf{u}_R + \mathbf{r}\times\mathbf{\Omega}\right)_R + \mathbf{\Omega}\times\left(\mathbf{u}_R + \mathbf{r}\times\mathbf{\Omega}\right) \tag{3.25}$$

Hence, accelerations in the two frames are relates as

$$\mathbf{a}_F = \mathbf{a}_R + 2\mathbf{\Omega}\times\mathbf{u}_R - \mathbf{\Omega}^2\mathbf{r} \tag{3.26}$$

The second term of the r.h.s is the Coriolis acceleration and the last term the centripetal acceleration. This last term is added to the Newtonian gravity as an effective gravity

$$\mathbf{g} = \mathbf{g_n} + \mathbf{\Omega}^2\mathbf{r} \tag{3.27}$$

The apparent force $\mathbf{\Omega}^2\mathbf{r}$ will be zero at the poles.

The momentum equations are now

$$\frac{\mathrm{D}\,\mathbf{u}}{\mathrm{D}\,t} = \mathbf{g} - \frac{1}{\rho}\nabla p + \nu\nabla^2\mathbf{u} - (2\mathbf{\Omega}\times\mathbf{u}) \tag{3.28}$$

It is clear that the Coriolis force $(-2\mathbf{\Omega}\times\mathbf{u})$ will deflect a particle to the right of its direction in the northern hemisphere (right-hand rule). As the Coriolis force constantly acts normal to the fluid path, it will not accelerate the particle (in fact, Coriolis does not play any role in the conservation of mechanical energy ...).

3.2.2 Thin shell approximation

A scale analysis of the continuity equation reveals that, for typical length scales much larger than typical vertical scales, $L \gg H$, horizontal velocities must be much larger than the vertical ones, $U \gg W$.

Now, decomposing the angular velocity vector into its three components (Fig.3.2), we have

$$\begin{aligned}\Omega_x &= 0\\ \Omega_y &= \Omega\cos\theta\\ \Omega_z &= \Omega\sin\theta\end{aligned}$$

The Coriolis term, assuming $U \gg W$, has the following components

$$2\mathbf{\Omega}\times\mathbf{u} = 2\Omega\left[(-v\sin\theta)\hat{i} + (u\sin\theta)\hat{j} - (u\cos\theta)\hat{k}\right] \tag{3.29}$$

and defining the Coriolis parameter as $f = 2\Omega\sin\theta$, which is now clearly twice the angular velocity and hence a (planetary) vorticity

$$2\mathbf{\Omega}\times\mathbf{u} = (-fv)\hat{i} + (fu)\hat{j} - (2\Omega u\cos\theta)\hat{k} \tag{3.30}$$

But the vertical component of the Coriolis force, $2\Omega u\cos\theta$, is negligible compared to the dominant terms in the vertical equation of motion, namely the pressure gradient and the gravitational acceleration. Our final set of momentum equations reduces to

$$\frac{\mathrm{D}\,u}{\mathrm{D}\,t} - fv = -\frac{1}{\rho}\frac{\partial p}{\partial x} + \nu\nabla^2 u \tag{3.31}$$

$$\frac{\mathrm{D}\,v}{\mathrm{D}\,t} + fu = -\frac{1}{\rho}\frac{\partial p}{\partial y} + \nu\nabla^2 v \tag{3.32}$$

$$\frac{\mathrm{D}\,w}{\mathrm{D}\,t} = -\frac{1}{\rho}\frac{\partial p}{\partial z} - g + \nu\nabla^2 w \tag{3.33}$$

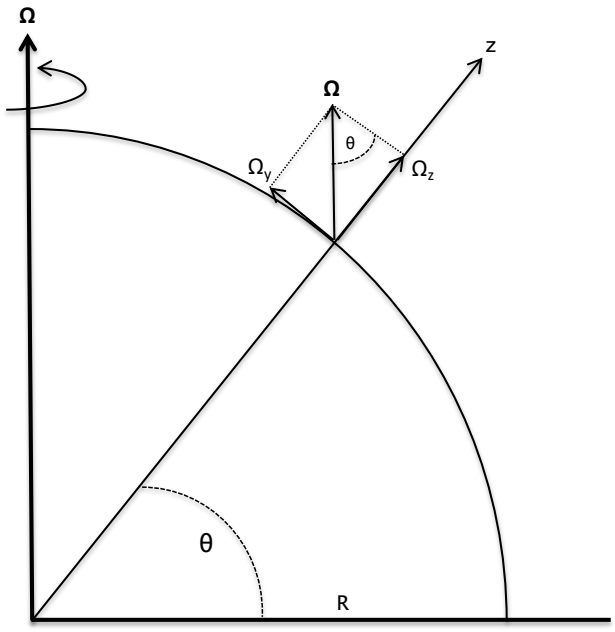

Figure 3.2: *Components of the angular velocity vector for a point on the sphere.*

Or

$$\boxed{\frac{\mathrm{D}\,\mathbf{u}}{\mathrm{D}\,t} + 2\boldsymbol{\Omega} \times \mathbf{u} = -\frac{1}{\rho}\nabla p - \mathbf{g} + \nu\nabla^2\mathbf{u}} \tag{3.34}$$

where $\nu = \mu/\rho$ is the kinematic viscosity.

3.2.3 The β-plane

A first approximation is to set the Coriolis parameter, f, to a constant value. This approximation, denoted the f-plane, is useful in some very idealized studies when the westward propagation of disturbances is not of interest or it is purposely neglected. But for large-scale dynamics it is not appropriate, when flows occurring over large horizontal scales are of interest. Rossby waves depend on variations of f, it is their restoring mechanism, for example, and the large-scale dynamics of the ocean will this be affected by latitudinal variations in the Coriolis parameter. An approximation can be done, however, to make equations more tractable, and it consists of considering a cartesian plane over which f does vary, so neglecting spherical coordinates.

The β-plane approximation is useful to avoid the sphericity and staying in a cartesian plane, yet retaining the dynamical effects of sphericity itself.

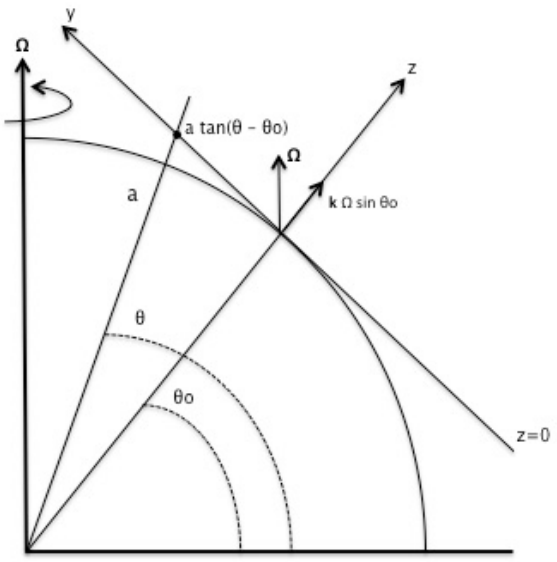

Figure 3.3: *A cartesian reference system (x,y,z) and its associated spherical system (r, θ, ϕ) around the point (a, θ_0, ϕ_0). The plane $z = 0$ (or β-plane) is tangent to the sphere around the point (a, θ_0, ϕ_0). The approximation $tan(\theta - \theta_0) \approx (\theta - \theta_0)$ is well justified for small variations in latitude. On the β-plane, the rotation vector is $\mathbf{k}\Omega\, sin\theta$, where $sin\theta \approx sin\theta_0 + (y/a)cos\theta_0$.*

The plane $z = 0$, what will be called the β-plane is tangent to the sphere in (a, θ_0, ϕ_0). For small variations in latitude we can approximate $tan(\theta - \theta_0) \approx \theta - \theta_0$. hence, our meridional cartesian coordinate is

$$\begin{aligned} y &= a(\theta - \theta_0) \\ z &= r - a \\ x &= (\phi - \phi_0) a\, cos\theta_0, \end{aligned}$$

where r is the distance of the fluid from the center of the sphere, θ is the latitude, ϕ the longitude, and a is the radius of the Earth.

Hence, latitude θ is a linear function of y

$$\theta = \theta_0 + \frac{y}{a}. \tag{3.35}$$

Now, for small variations in latitude we have:

$$sin\theta \approx sin\theta_0 + cos\theta_0 \frac{y}{a}, \tag{3.36}$$

as a truncated series around θ_0. And we can express f as the following:

$$f = 2\Omega sin\theta = 2\Omega sin\theta_0 + \frac{2\Omega}{a} cos\theta_0\, y = f_0 + \beta\, y. \tag{3.37}$$

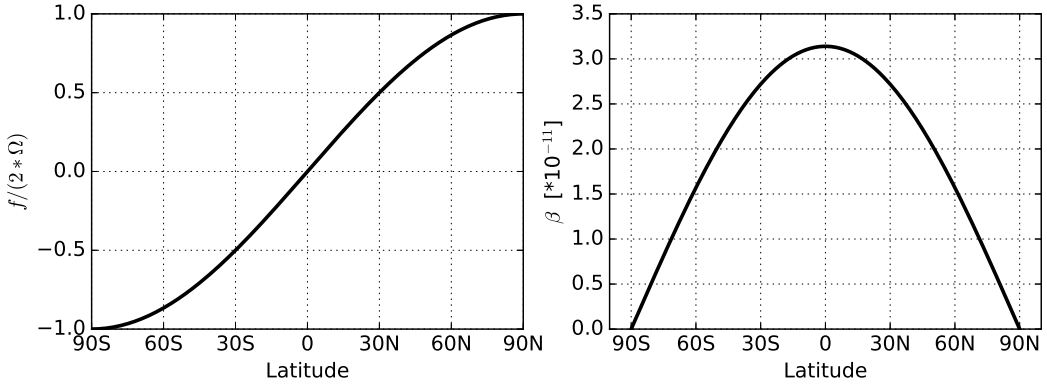

Figure 3.4: *The Coriolis parameter f and its meridional gradient β as a function of latitude.*

Where we have introduced $\beta = \frac{2\Omega}{a} cos\theta_0$.

But what is β? We have gone from $f = 2\Omega sin\theta$ to $f = f_0 + \beta y$. The dependence of f on latitude is conserved because of the linear relationship between f and y. This is an important result: **we are not working on spherical coordinates but the dynamical effects of sphericity are retained.**

β is called the gradient of planetary vorticity given that:

$$\frac{\partial f}{\partial y}(\theta = \theta_0) = \frac{1}{a}\frac{\partial f}{\partial \theta}(\theta = \theta_0) = \frac{2\Omega}{a} cos\theta_0 = \beta. \tag{3.38}$$

Typical mid-latitude values for f and β are 10^{-4} s^{-1} and 10^{-11} m^{-1}s^{-1} (Fig. 3.4).

In conclusion, we have the β-plane approximation as

$$\boxed{f = f_0 + \beta y} \tag{3.39}$$

For relatively large areas, with θ varying over a few tens of degrees, between mid-latitudes and the equator, the tangent plane approximation is called β-plane. This approximation is only valid if

$$\beta y \ll f_0 \quad or \quad \frac{\beta y}{f_0} \ll 1. \tag{3.40}$$

For even smaller variations in θ the f-plane is used, where

$$f = f_0 = 2\Omega\, sin\theta_0. \tag{3.41}$$

3.3 Kinematical and dynamical approximations

3.3.1 Hydrostatic balance

The vertical component (the component parallel to the gravitational force, **g**) of the momentum equation is

$$\frac{\mathrm{D}\, w}{\mathrm{D}\, t} = -\frac{1}{\rho}\frac{\partial p}{\partial z} - g, \tag{3.42}$$

where w is the vertical component of the velocity and $\mathbf{g} = -g\mathbf{k}$. If the fluid is static the gravitational term is balanced by the pressure term and we have

$$\frac{\partial p}{\partial z} = -\rho g, \tag{3.43}$$

which is called the *hydrostatic balance*, or hydrostasy. Scaling analysis shows that the hydrostatic balance is the dominant balance within the vertical momentum equation , so long as the vertical length scales of motion are much smaller than the horizontal length scales. Such scales are relevant for large-scale ocean climate modeling, and global ocean models typically assume a hydrostatic balance, and this constitutes a basic assumption of the primitive equations. Integrating the hydrostatic balance vertically from the ocean surface η determines the pressure at a point in the ocean column

$$p(z) = p_a + g\int_z^\eta \mathrm{d}z' \rho(z'), \tag{3.44}$$

where p_a is the sea surface pressure resulting from external forcing (e.g., atmospheric loading, sea ice, ...).

Scaling and aspect ratio

For a Boussinesq fluid, the momentum equations are

$$\frac{\mathrm{D}\,\mathbf{u}}{\mathrm{D}\, t} + \mathbf{f}\times\mathbf{u} = -\nabla\phi \tag{3.45}$$

$$\frac{\mathrm{D}\, w}{\mathrm{D}\, t} = -\frac{\partial\phi}{\partial z} + b, \tag{3.46}$$

where $\phi = p/\rho_0$ and buoyancy $b = -g\rho/\rho_0$. In the case of $f = 0$ the horizontal momentum equation reduces to

$$\frac{\mathrm{D}\,\mathbf{u}}{\mathrm{D}\, t} = -\nabla\phi \tag{3.47}$$

and a scaling for the horizontal equation is

$$\frac{U}{T} \sim \frac{\Phi}{L}, \text{or} \frac{LU}{T} \sim \Phi, \text{or} U^2 \sim \Phi. \tag{3.48}$$

Using mass conservation to scale vertical velocities we obtain

$$\nabla_z \cdot \mathbf{u} + \frac{\partial w}{\partial z} = 0. \tag{3.49}$$

A scaling of this equation is

$$\frac{U}{L} + \frac{W}{H} = 0 \tag{3.50}$$

$$W = \frac{H}{L} U = \alpha U \tag{3.51}$$

where $\alpha \equiv \frac{H}{L}$ is the aspect ratio between the typical horizontal and vertical scales. The advective terms in the vertical momentum equation scale as

$$\frac{\mathrm{D}w}{\mathrm{D}t} \sim \frac{W}{T} = \frac{U}{L} W = \frac{U}{L} (\frac{H}{L} U) = \frac{U^2 H}{L^2}. \tag{3.52}$$

Now we can use the scaling for the horizontal and vertical motions, together with the aspect ratio of their typical scales, to reveal the condition for hydrostasy.

For hydrostatic balance to hold, the ratio of advective terms to the pressure gradient term in (3.46) must be

$$\frac{|\frac{\mathrm{D}w}{\mathrm{D}t}|}{|\frac{\partial \phi}{\partial z}|} \ll 1 \tag{3.53}$$

This implies that

$$\frac{|\frac{\mathrm{D}w}{\mathrm{D}t}|}{|\frac{\partial \phi}{\partial z}|} \sim \frac{U^2 H / L^2}{U^2 / H} \sim \left(\frac{H}{L}\right)^2 \ll 1. \tag{3.54}$$

In other words, the aspect ratio should be

$$\alpha^2 \equiv \left(\frac{H}{L}\right)^2 \ll 1 \tag{3.55}$$

for the advective terms in the vertical momentum to be neglected. The hydrostatic balance is then a *small aspect ratio approximation*.

3.3.2 Hydrostatic approximation

3.3.3 Shallow water approximation

3.3.4 Boussinesq approximation

3.3.5 Rigid lid approximation

3.4 Rossby number

We consider the dynamical balance in the horizontal components of the momentum equation. In the horizontal plane (along geopotential surfaces) we find that the Coriolis term is much larger than the advective terms and the dominant balance is between Coriolis and the horizontal pressure force. The balance is called *geostrophic balance*, and it occurs when the Rossby number is small.

The horizontal momentum equation is

$$\frac{\partial \mathbf{u}}{\partial \mathbf{t}} + (\mathbf{v} \cdot \nabla)\mathbf{u} + \mathbf{f} \times \mathbf{u} = -\frac{1}{\rho}\nabla_z p, \tag{3.56}$$

where $\mathbf{v} = (u, v, w)$ and $\mathbf{u} = (u, v, 0)$. A scaling analysis of the second (U^2/L) and third (fU) terms, where U is the approximate magnitude of the horizontal velocities and L is a typical length scale over which that velocity varies, reveals the importance of rotation. The ratio of the sizes of the advective and Coriolis terms defines the Rossby number:

$$\boxed{Ro \equiv \frac{U}{fL}} \tag{3.57}$$

The Rossby number characterizes the importance of rotation in a fluid. It is the ratio of the magnitude of the relative acceleration to the Coriolis acceleration, and it is of fundamental importance in geophysical fluid dynamics.

3.5 Geostrophic and Thermal Wind Balance

If the Rossby number is sufficiently small, then the rotation term dominates the nonlinear advection term, and if the time period of the motion scales advectively (or there are no accelerations) then the rotation term also

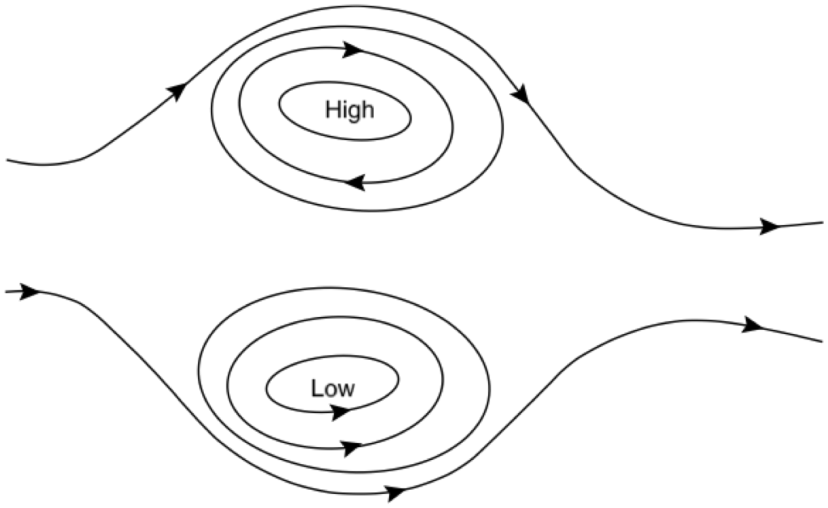

Figure 3.5: Schematic of a geostrophically balanced flow with a positive value of the Coriolis parameter f. Flow is parallel to the lines of constant pressure. Cyclonic flow is anticlockwise around a low pressure region. [from *Vallis* (2006)]

dominates the local time derivative. The only term that can then balance the rotation term is the pressure term, leaving us with

$$fv \approx \frac{1}{\rho}\frac{\partial p}{\partial x} \tag{3.58}$$

$$fu \approx -\frac{1}{\rho}\frac{\partial p}{\partial y}. \tag{3.59}$$

This balance is known as *geostrophic balance*, and is one of the pillars of geophysical fluid dynamics. We can now define geostrophic velocities as

$$fu_g = -\frac{1}{\rho}\frac{\partial p}{\partial y} \qquad fv_g = \frac{1}{\rho}\frac{\partial p}{\partial x} \tag{3.60}$$

and for flows with a low Rossby numbers, $u \approx u_g$ and $v \approx v_g$.

A geostrophic flow is parallel to lines of constant pressure (isobars). If $f > 0$, after a pressure gradient is initiated somehow, the fluid starts to move down the gradient. Then, the fluid experiences the Coriolis force to the right and therefore swings to the right. The fluid eventually moves along isobars (along the slope, not down it), with the pressure force down

the slope balanced by the Coriolis force up the slope. In the northern hemisphere, the flow is anticlockwise round a region of low pressure and clockwise around a region of high pressure.

Consider now a plane horizontal flow in which density does not vary along the fluid path (the Boussinesq approximation). In this case the continuity equation reduces to

$$\frac{\partial u}{\partial x} + \frac{\partial v}{\partial y} = 0. \tag{3.61}$$

We can now define a function $\psi(x, y, t)$ such that

$$u \equiv -\frac{\partial \psi}{\partial y}, \tag{3.62}$$

$$v \equiv \frac{\partial \psi}{\partial x}, \tag{3.63}$$

and Eq.3.61 is thus satisfied, and this is called a *streamfunction*.

Returning to our geostrophic balance, if the Coriolis force is constant and if density does not vary in the horizontal, the geostrophic flow is horizontally non-divergent

$$\nabla_z \cdot \mathbf{u_g} = \frac{\partial u_g}{\partial x} + \frac{\partial v_g}{\partial y} = 0, \tag{3.64}$$

and we may define a geostrophic streamfunction, ψ_g, by $\psi_g \equiv \frac{p}{f\rho}$, and

$$u_g \equiv -\frac{\partial \psi}{\partial y}, \quad v_g \equiv \frac{\partial \psi}{\partial x}. \tag{3.65}$$

Thermal wind

Thermal wind balance arises when combining the geostrophic and hydrostatic approximations. They are useful in elucidating how temperature differences in the horizontal can lead to vertical variations in geostrophic velocities, hence the term *thermal wind equations*.

Taking the vertical derivative of the geostrophic equations for a Boussinesq fluid

$$\rho_0 f \partial_z u = -\partial_z \frac{\partial p}{\partial y} \tag{3.66}$$

$$\rho_0 f \partial_z v = \partial_z \frac{\partial p}{\partial x}. \tag{3.67}$$

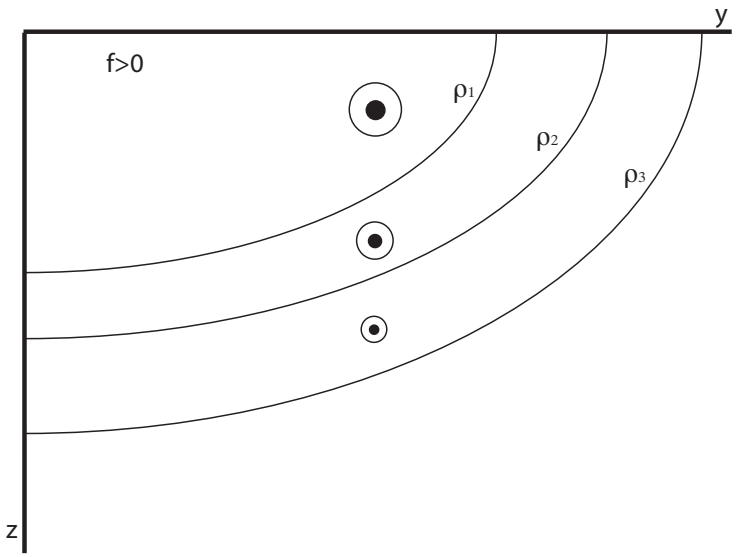

Figure 3.6: Schematic of thermal wind balance in the northern hemisphere. Shown are surfaces of constant density, or isopycnals. Density increases with depth and latitude, $\rho_3 > \rho_2 > \rho_1$. The termal wind associated with this density field is eastward, or out of the page, and decreases with depth. The same eastward thermal wind velocity would have resulted in the southern hemisphere, with $\rho_y < 0$ and $f < 0$.

Combining these with the hydrostatic balance, $\partial_z p = -\rho g$, and changing the order of differentiation for p, gives

$$\rho_0 f \, \partial_z u = g \, \partial_y \rho \tag{3.68}$$
$$\rho_0 f \, \partial_z v = -g \, \partial_x \rho. \tag{3.69}$$

These equations represent the *thermal wind balance*, and the vertical derivative of the geostrophic wind is the 'thermal wind'. Thermal wind balance says that **the geostrophic velocity has a vertical *thermal wind shear* in case where density has a horizontal gradient**.

In general, zonally averaged ocean temperature decrease poleward due to the differential heating received from solar radiation. Neglecting salinity effects on density, this poleward reduction in temperature corresponds to a poleward increase in density. Also, for a stably stratified fluid, density increases with depth. In a zonally-averaged flow, $\partial_x \rho = 0$, and so thermal wind reduces to

$$\partial_z u = \frac{g}{\rho_0 f} \, \partial_y \rho \tag{3.70}$$

This equation is telling us that, if temperature falls in the poleward direc-

tion, $\partial_y \rho > 0$, then the zonally-averaged thermal wind is eastward. Wind shear also increases as we move upward in the ocean, $\partial_z u > 0$, which yields a surface intensified zonal velocity field. Thermal wind, although diagnostic, represents a valid steady state balance of a frictionless rotating fluid. That is, in the presence of rotation, a flow can exist in steady state with nonflat isopycnals. Vertical integration of the thermal wind relation, along with knowledge of the geostrophic velocity at a point along the integration path, allows for determination of the full geostrophic velocity in terms of density. However, the baroclinic density field (with a horizontal gradient) is related to the baroclinic component of the velocity field through thermal wind balance. The barotropic flow component has zero vertical shear.

3.6 The Rossby radius

The Rossby radius of deformation is a length scale of fundamental importance in atmosphere-ocean dynamics. It describes the horizontal scale at which rotation effects become as important as buoyancy effects. For example, in the first stage of an adjustment problem, first the disturbance has a small structure and gravity dominates with a very large pressure gradient. Later, as the perturbation spreads over a larger horizontal scale, Coriolis becomes more important and of similar magnitude as the pressure gradient, and thus rotation causes a response that is much different from a non-rotating case.

Using a geostrophic flow, it is easy to show that the Rossby radius of deformation, L_d, is

$$L_d = c/|f| = (gH)^{1/2}/|f| \tag{3.71}$$

where c is the phase speed of the gravity wave. For the deep ocean, where H= 4 km and c= 200 m/s, the Rossby radius is about 2000 km. Which is much larger than depth, so the hydrostatic approximation is valid. However, the ocean is not only in rotation but also stratified, and so what is more important is not the barotropic radius of deformation but rather the baroclinic ones

$$L_d = c_n/|f| \tag{3.72}$$

where c_n are baroclinic gravity wave phase speeds. So the Rossy radius is directly related to the phase speed of long, baroclinic gravity waves, which is also a very useful parameter in the study of ocean wave dynamics. A global atlas of the first baroclinic gravity-wave phase speed, c, has been

computed on a 1-degree global grid from observations (Fig. 3.7) as follows

$$c_n \sim \frac{1}{n\pi} \int_{-H}^{0} N \, \mathrm{d}z \tag{3.73}$$

where N is the buoyancy frequency.

Now, the first baroclinic Rossby radius, given that c_1=1-3 m/s, is L_d ∼10-30 km with values increasing towards low latitudes (Fig. 3.8). Mesoscale eddies have the size of the first baroclinic Rossby radius, therefore in order to resolve mesoscale eddies and associated fluxes, ideally an ocean model should have at least two grid points within L_d. It is clear from Fig. 3.9 that standard global ocean model can resolve mesoscale fluxes up to ∼25°, poleward of that latitude fluxes need to be parameterized. Benefits of having fine-resolution ocean models is illustrated in Fig. 3.10, where eddies and filaments are ubiquitous in the fine-resolution version of the model whereas a laminar ocean is simulated in the (standard!) 1° version.

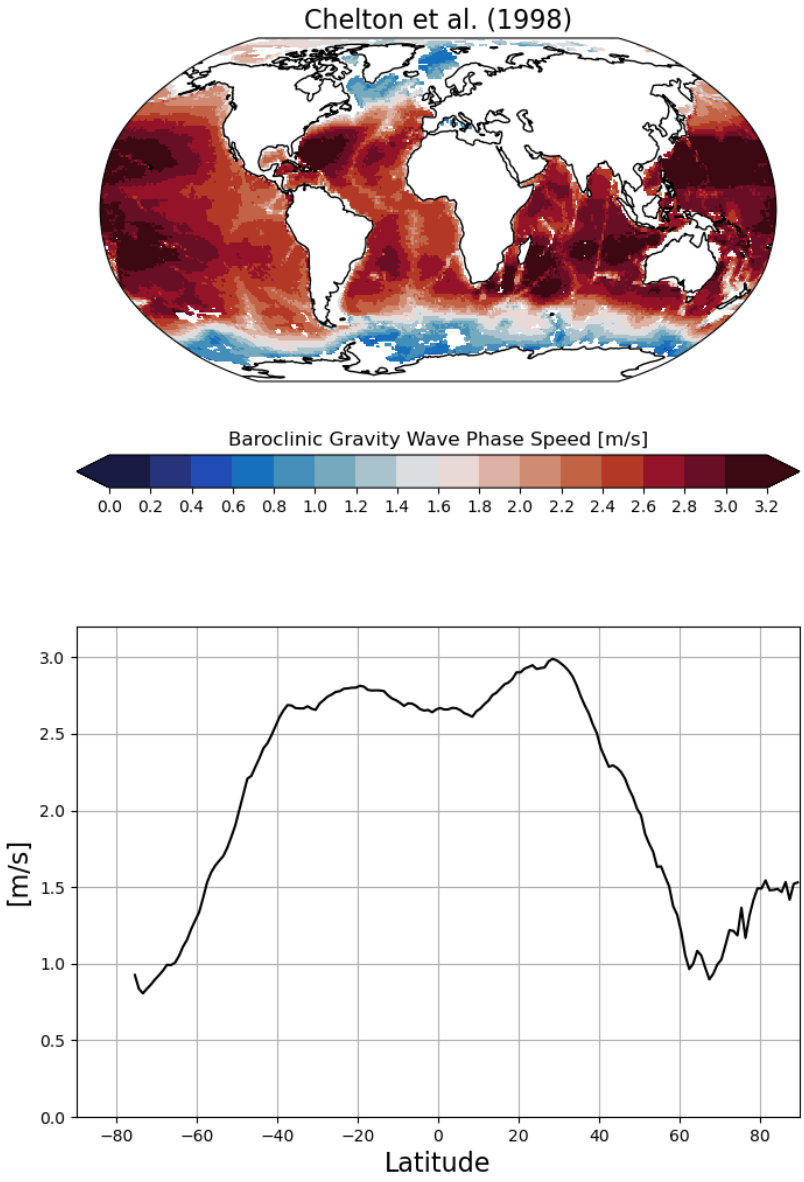

Figure 3.7: A global map of the first baroclinic gravity wave phase speed and its zonal mean. [data from Chelton et al., 1998]

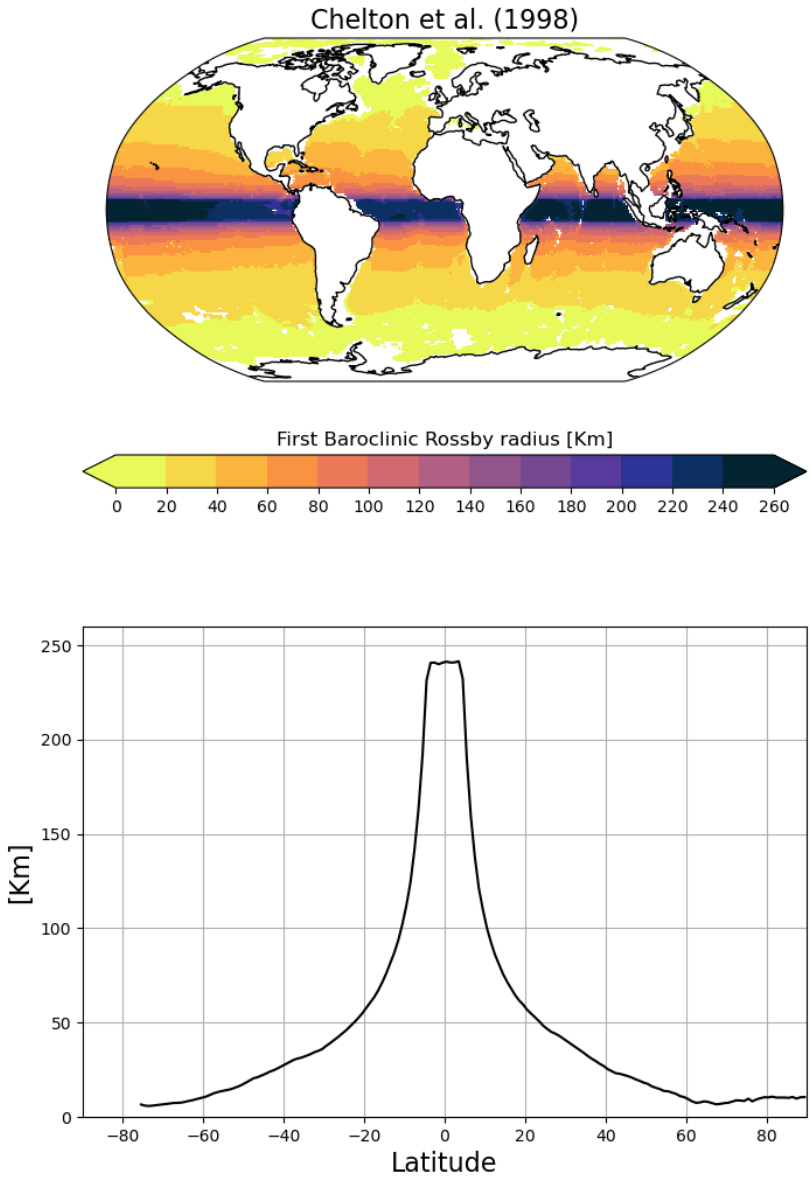

Figure 3.8: A global map of the first baroclinic Rossby radius of deformation and its zonal mean. [data from Chelton et al., 1998]

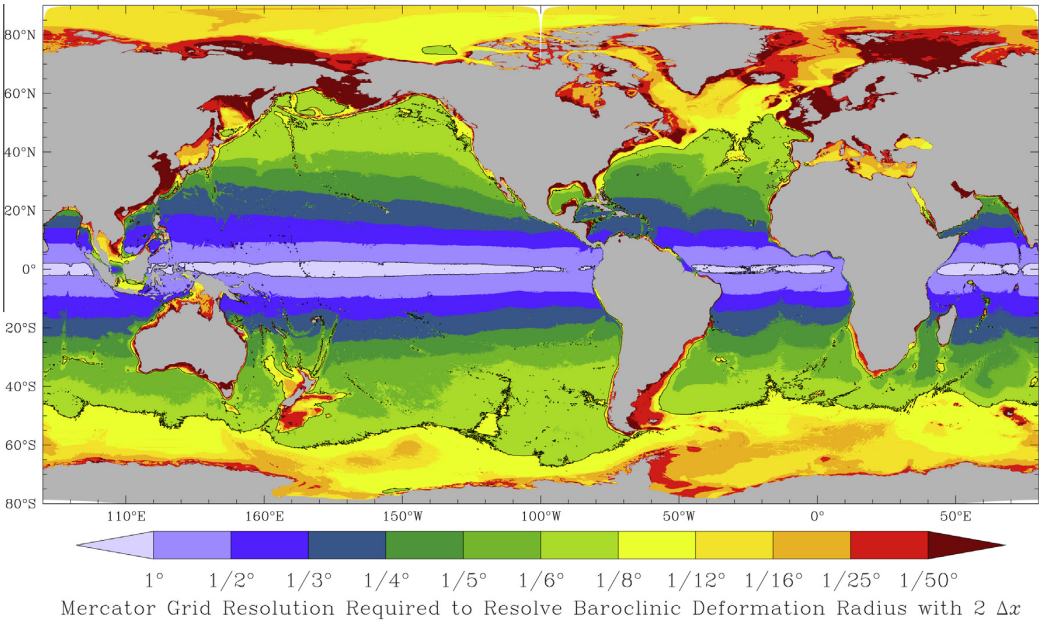

Figure 3.9: The oceanic resolution needed to resolve the Rossby Radius of deformation in an ocean model [from Hallberg et al., 2013].

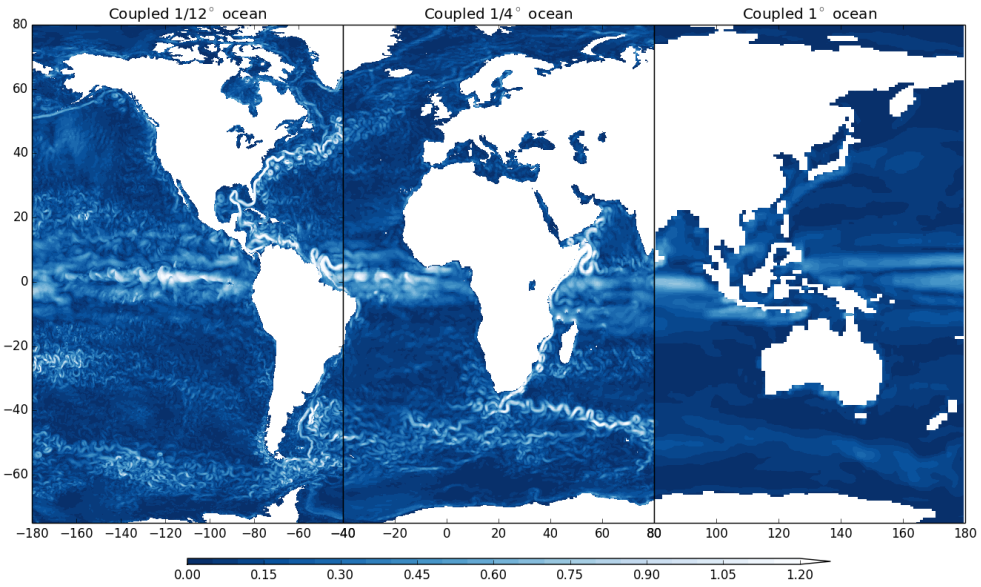

Figure 3.10: The same ocean model at different horizontal resolutions, increasing from right to left.

Let's now go a little ahead of ourselves. Consider that the Coriolis parameter is not constant and is actually a function of latitude $f(y)$. The nondivergent condition $\nabla \cdot (f\mathbf{u}) = 0$ is satisfied by the geostrophically balanced flow. Cross-differentiating Eq.3.60 gives

$$\frac{\partial f}{\partial y} v_g + f \nabla_z \cdot \mathbf{u_g} = 0 \tag{3.74}$$

Using mass continuity leads to

$$\boxed{\beta v_g = f \frac{\partial w}{\partial z}}, \tag{3.75}$$

where $\beta \equiv \frac{\partial f}{\partial y}$. This is a geostrophic vorticity balance, also called *S*verdrup balance. In a Sverdrup balance, the vertical velocity results from an external agent, most notably wind stress. It states that the vertical shear in the vertical velocity balances a meridional current, with the Coriolis parameter f and the planetary vorticity gradient β determining the sense and strength of the meridional flow. A vertical velocity shear arises when there is a nonzero curl in the wind stress acting on the ocean surface. Vorticity is then transferred to the ocean via frictional effects causing *Ekman pumping or suction*. These effects alter the vertical structure of the vertical velocity and, through Sverdrup balance, induce a meridional flow.

3.7 The shallow-water equations

To describe large-scale oceanic, and atmospheric, motions, where the horizontal scale is much larger than the vertical scale, we can use a set of simplified equations that retain the necessary ingredients of the fluid motion but use some useful approximations. We will thus consider a fluid in hydrostatic balance of constant density and, for simplicity, we will also consider a flat bottom. The necessary condition of the shallow-water equations is that the horizontal length scale must be much larger than the vertical scale over which the fluid develops so that $L >> H$.

If the fluid is in hydrostatic balance

$$\frac{\partial p}{\partial z} = -\rho g. \tag{3.76}$$

Then the total pressure will be

$$p(x, y, z, t) = -\rho g z + p'. \tag{3.77}$$

Pressure must vanish at the surface, so that $p = 0$ at $z = \eta$

$$p = p_0 + p' = 0 \tag{3.78}$$

and at $z = \eta$ we have

$$p' = \rho g \eta \tag{3.79}$$

Our total pressure will then be

$$p(x, y, z, t) = \rho g(\eta(x, y) - z) \tag{3.80}$$

This means that the horizontal gradient of pressure, and the flow, is independent of depth

$$\nabla p = \rho g \nabla \eta \tag{3.81}$$

and the horizontal momentum equations reduce to

$$\frac{\mathrm{D}\,\boldsymbol{u}}{\mathrm{D}\,t} = -\frac{1}{\rho}\nabla p = -g\nabla\eta \tag{3.82}$$

We can now easily add rotation to our shallow-water momentum equations

$$\boxed{\frac{\mathrm{D}\,\boldsymbol{u}}{\mathrm{D}\,t} + \boldsymbol{f} \times \boldsymbol{u} = -\frac{1}{\rho}\nabla p = -g\nabla\eta} \tag{3.83}$$

The continuity equation is obtained by the mass balance within an infinitesimal column of fluid. The mass flux passing through a section of the

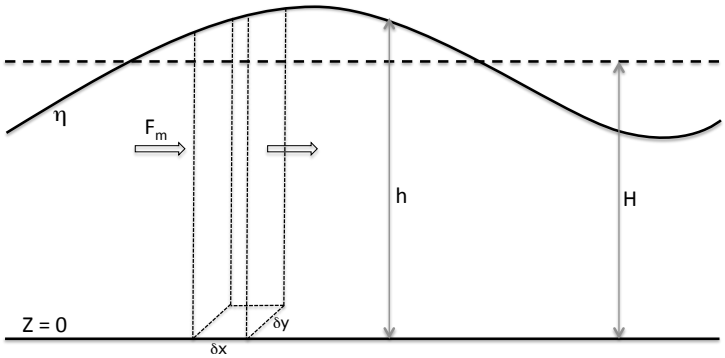

Figure 3.11: Schematic of a flat-bottomed shallow-water system and mass balance within a column of fluid.

column is $F_m = \rho u(H+\eta)\delta y$ and the difference between the fluxes into and out of the section is given by

$$\delta x \delta y \frac{\partial}{\partial x}[\rho u(H+\eta)] \tag{3.84}$$

Considering the total volume, the net rate of change is

$$\frac{\partial h}{\partial t} + \frac{\partial}{\partial x}[u(H+\eta)] + \frac{\partial}{\partial y}[v(H+\eta)] = 0 \tag{3.85}$$

which is the new continuity equation for the shallow-water system

$$\frac{\partial h}{\partial t} + \frac{\partial}{\partial x}(uh) + \frac{\partial}{\partial y}(vh) = 0 \tag{3.86}$$

$$\boxed{\frac{\partial h}{\partial t} + \nabla \cdot (\boldsymbol{u}h) = 0} \tag{3.87}$$

and if the perturbation is small and H is constant, mass continuity reduces to the linear equation

$$\boxed{\frac{\partial \eta}{\partial t} + \mathrm{H}\nabla \cdot \boldsymbol{u} = 0} \tag{3.88}$$

If there is flux by advection this is balanced by a net increase in mass and an increase in height, giving rise to a vertical velocity, so that the mass convergence is balanced by the increase in height allowing for a dynamical surface elevation. This will be the basis for the propagation of waves within the rotating shallow-water system.

Exercices

1. Use $\phi = p/\rho_0$ and the definition of buoyancy $b = -g\rho/\rho_0$ to rewrite the hydrostatic balance and thermal wind equations.

2. Where is thermal wind velocity directed in the southern hemisphere, considering a poleward increasing (decreasing) density (temperature)? (see Fig. 3.12)

3. How is thermal wind shear changed as we approach the poles?

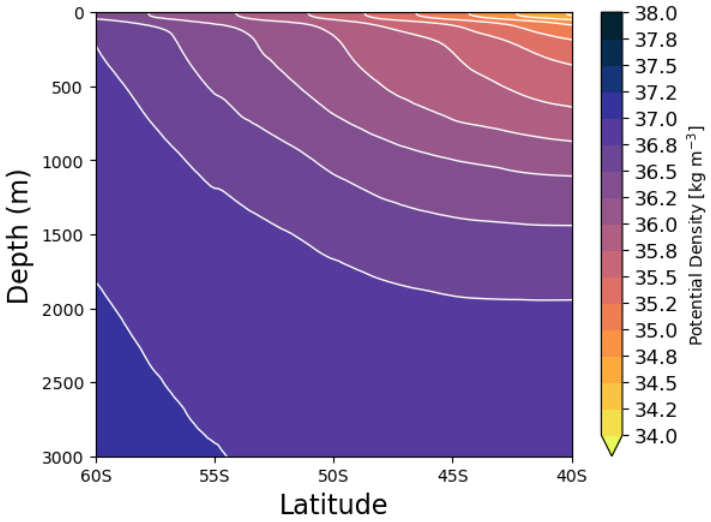

Figure 3.12: Zonal-mean potential density in the latitudes of the Drake Passage.

Chapter 4

Waves in the ocean

In this chapter we describe the general solution and dynamics of shallow-water waves and try to put them into a wider context, emphasizing their role in the ocean circulation and the coupled ocean-atmosphere system.

We will look for wave solutions of the shallow-water equations on the f-plane and β-plane. A few solutions will appear, some have already been discussed in different contexts, and some are new.

4.1 Poincaré Waves

We start by linearizing our shallow-water equations for a fluid $h = H + \eta$ over a state at rest

$$\boldsymbol{u} = u' \tag{4.1}$$
$$h = H + \eta \tag{4.2}$$

so that our equations, after eliminating higher order terms, reduce to

$$\frac{\partial u}{\partial t} - f_0 v = -g\frac{\partial \eta}{\partial x} \tag{4.3}$$
$$\frac{\partial v}{\partial t} + f_0 u = -g\frac{\partial \eta}{\partial y} \tag{4.4}$$
$$\frac{\partial \eta}{\partial t} + H\nabla \cdot \boldsymbol{u} = 0 \tag{4.5}$$

A dispersion relation can now be obtained by looking for wave solutions of the type

$$(u, v, \eta) = (u_0, v_0, \eta_0)e^{i(kx+ly-\omega t)} \tag{4.6}$$

into our linearized equations:

$$\begin{aligned} -u_0 i\omega - f_0 v_0 &= -g\eta_0 ik & (4.7)\\ -v_0 i\omega + f_0 u_0 &= -g\eta_0 il & (4.8)\\ -\eta_0 i\omega + H(iku_0 + v_0 il) &= 0 & (4.9) \end{aligned}$$

Non-trivial solutions of the system exist only if the determinant is equal to zero, so that

$$\begin{vmatrix} -i\omega & -f_0 & gik \\ f_0 & -i\omega & gil \\ ikH & ilH & i\omega \end{vmatrix} = 0 \tag{4.10}$$

and this is true if

$$\omega[\omega^2 - f_0^2 - gH(k^2 + l^2)] = 0 \tag{4.11}$$

Now, there are a few interesting possible solutions for the frequency ω.

The first case is $\omega = 0$. This solution describes a time-independent flow and the equations describe a geostrophically balanced flow.

The second possible solution is if

$$\boxed{\omega^2 = f_0^2 + c^2(k^2 + l^2)} \tag{4.12}$$

where $c = (gH)^{1/2}$ is the gravity wave phase speed. The dispersion relation describes wave solutions of superinertial flow ($\omega > f_0$) which are called Poincaré waves. From this solution we can highlight three possible limiting cases (see Fig. 4.1).

First, the limit of no rotation, when $f_0 = 0$. The solution reduces to $\omega^2 = c^2K^2$ and the frequency solutions are

$$\boxed{\omega = \pm Kc} \tag{4.13}$$

where $K = (k^2 + l^2)$, which describe a classical gravity wave.

Second, the short wave limit, when $K^2 \gg f_0^2/(gH)$, which gives

$$\boxed{\omega^2 = c^2K^2} \tag{4.14}$$

again, the dispersion relation is that of the non-rotating case with phase speed c. This is because

$$\frac{2\pi^2}{\lambda^2} \gg \frac{f^2}{gH} \quad \frac{2\pi}{\lambda} \gg \frac{f}{c} \quad \lambda \ll \frac{(gH)^{1/2}}{f} 2\pi \tag{4.15}$$

so that $L_d \gg \lambda$, where L_d is the Rossby radius $L_d = (gH)^{1/2}/f$. Basically, this solution looks like a gravity wave in a rotating case.

Third, the long wave limit, when $K^2 \ll f_0^2/(gH)$. In this case we have

$$\boxed{\omega^2 = f_0^2} \tag{4.16}$$

and therefore the Rossby radius is much smaller than the wave length, $L_d \ll \lambda$. In this limiting case, there is no space dependency, $k = l = 0$, and the surface elevation anomaly is also zero $\eta = 0$. The solution is

$$\frac{\partial u}{\partial t} - fv = 0 \tag{4.17}$$

$$\frac{\partial v}{\partial t} + fu = 0 \tag{4.18}$$

and these are called inertial oscillations, circulating at the planetary frequency $\omega = f$.

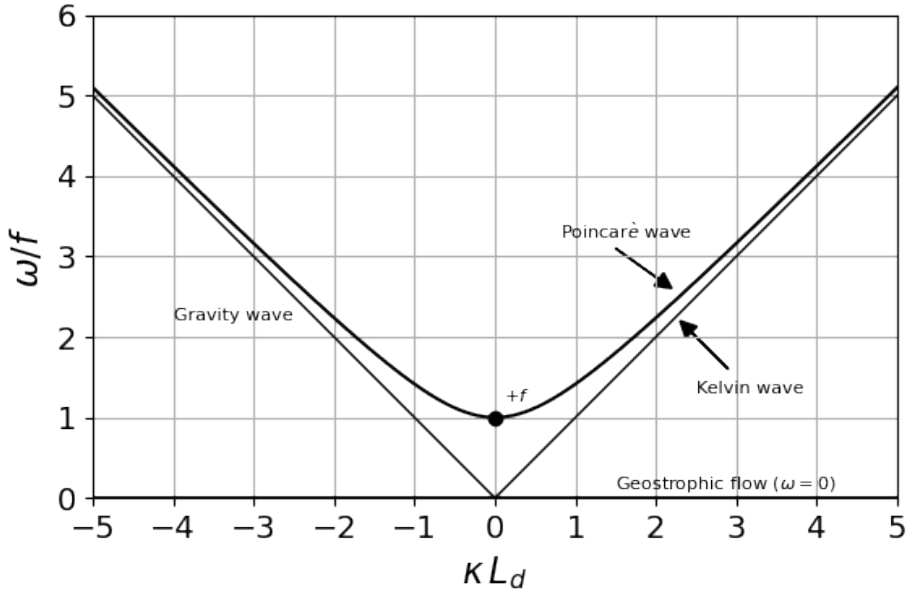

Figure 4.1: *Dispersion relation for Poincarè and Kelvin waves. The frequency is scaled by f and the wavenumber by L_d. The black dot marks the inertial oscillations regime and the $\omega = 0$ is the geostrophic case.*

4.2 Kelvin Waves

Kelvin waves are a particular solution of the shallow water equations describing a gravity wave that exists in a rotating frame and with the help of lateral boundaries. We could show Kelvin waves propagating in a channel, with two parallel boundaries, but for a start we will consider the case of a single lateral boundary. The first assumption is that, if $u = 0$ at the boundary, we could simply consider the zonal component of the velocity zero everywhere. The meridional component is not zero at the boundary, because the flow is frictionless. The linearized shallow water equations are

$$-f_0 v = -g\frac{\partial \eta}{\partial x} \tag{4.19}$$

$$\frac{\partial v}{\partial t} = -g\frac{\partial \eta}{\partial y} \tag{4.20}$$

$$\frac{\partial \eta}{\partial t} + H\frac{\partial v}{\partial y} = 0 \tag{4.21}$$

Continuity becomes

$$\frac{\partial \eta}{\partial t \partial y} = -H\frac{\partial^2 v}{\partial y^2} \tag{4.22}$$

and using the momentum equation

$$\frac{\partial^2 v}{\partial t^2} = gH\frac{\partial^2 v}{\partial y^2} \tag{4.23}$$

which is the standard wave equation with phase speed $c = (gH)^{1/2}$. The solution to this is

$$v = V_1 \cos k(y - ct) + V_2 \cos k(y + ct) \tag{4.24}$$

and the wave propagates along the meridional boundary. Substituting this solution into the momentum equation we obtain a solution for η

$$\eta = V_1 \frac{c}{g} \cos k(y - ct) - V_2 \frac{c}{g} \cos k(y + ct) \tag{4.25}$$

which describes a propagating wave in terms of surface elevation. The solution has been found for both v and η with no Coriolis term: this has the characteristics of a non-rotating shallow water wave. The velocity is in geostrophic balance with the pressure field, although it is a wave and $\omega \sim f$.

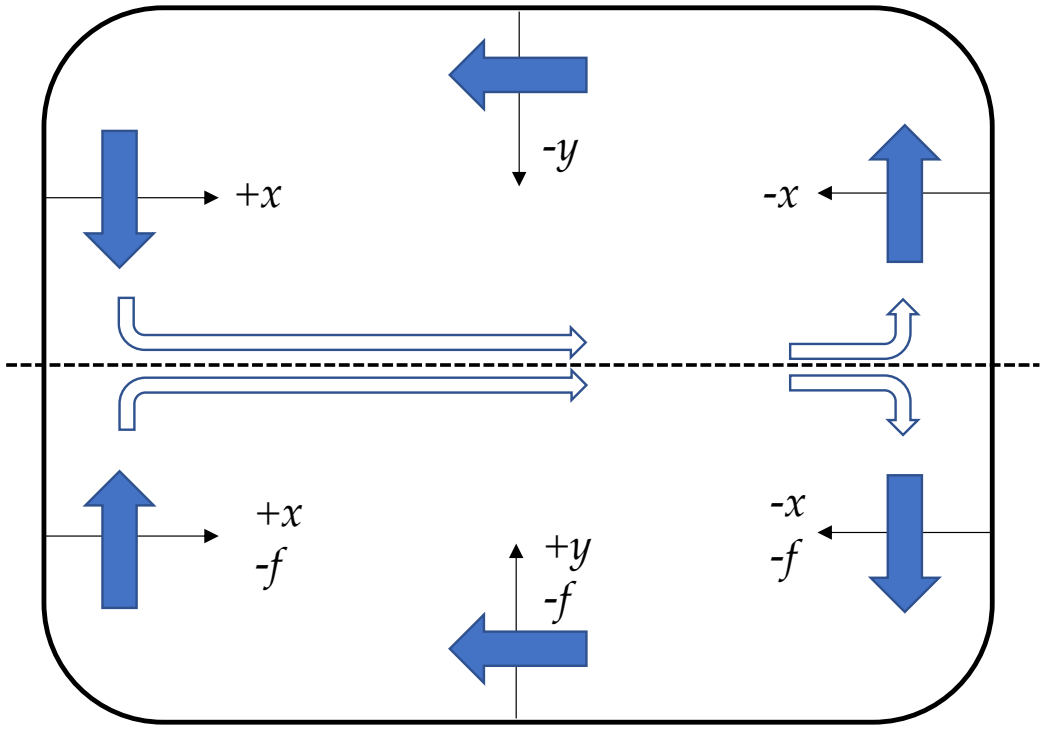

Figure 4.2: *For a system bounded to the west (x positive) the wave propagates in the negative y direction, i.e. to the south. If x is negative this reverses so on the eastern side of the basin the Kelvin wave propagates northwards. In the northern hemisphere a Kelvin wave will keep the coast to its right as it pushed against it by the Coriolis force.*

The solutions in the x-direction are

$$V_1 = e^{f_0/cx} \tag{4.26}$$

$$V_2 = e^{-f_0/cx} \tag{4.27}$$

and remember that $f_0/c = L_d^{-1}$. The first solution grows exponentially for positive x away from the meridional boundary, which is not physically possible. We are then left with the following set of solutions

$$v = e^{-x/L_d} \cos k(y + ct) \tag{4.28}$$

$$u = 0 \tag{4.29}$$

$$\eta = -e^{-x/L_d} \frac{c}{g} \cos k(y + ct) \tag{4.30}$$

$$= -(H/g)^{1/2} e^{-x/L_d} \cos k(y + ct) \tag{4.31}$$

These are Kelvin waves. They are trapped by the meridional boundary and decay exponentially away from it. The trapping spatial scale is given

by the Rossby radius, and for f_0 positive the boundary is at the right of the wave propagation. Kelvin waves are balancing f against the wall, which could be a topographic boundary or a waveguide such as the equator (Fig. 4.2).

Barotropic Kelvin waves are also tidal waves, propagating around an amphidromic point .

4.3 Planetary, or Rossby, waves

The time-dependent ocean circulation has an important impact on our climate due to the ocean large heat capacity. Any abrupt change, the intrinsic variability and possible variations of the general circulation caused by the atmospheric influence is fundamental in climate studies. Moreover, the oceans are no longer considered passive in the atmosphere-ocean system, but contribute to the production of the climate low-frequency variability at interannual to decadal time scales (*Talley*, 1999; *Dewar*, 2001; *Pierce et al.*, 2001).

The oceans are forced at the surface by the wind frictional stress and Rossby waves appear to play a fundamental role in redistributing and dispersing large-scale time-varying energy in the ocean. The propagation of Rossby waves towards the ocean interior under the influence of wind stress results in establishing a Sverdrup balance in the basin, accumulating energy in the western boundaries and intensifying currents there (*Anderson and Gill*, 1975, 1979).

Due to the ubiquitous presence of Rossby waves in the world oceans they influence ocean gyres and air-sea fluxes at all latitudes, affecting in turn the atmospheric heat transport and circulation. They are believed to provide teleconnections between the equatorial and middle latitudes regions (*Galanti and Tziperman*, 2003) as well as transhemispheric and interbasin communications (*Cessi and Otheguy*, 2003). Other major effects are the maintenance and intensification of western boundary currents, transport of a large amount of heat and, because of their time-scale, they play a key role in the climate system.

Rossby waves are very long waves so that the f-plane is not a good approximation anymore and we will build our solutions on the β-plane. The frequency is going to be subinertial, $\omega \ll f$, and so they are close to geostrophy.

Our set of equations is

$$\frac{\partial u}{\partial t} - (f_0 + \beta y)\, v = -g\frac{\partial \eta}{\partial x} \tag{4.32}$$

$$\frac{\partial v}{\partial t} + (f_0 + \beta y)\, u = -g\frac{\partial \eta}{\partial y} \tag{4.33}$$

$$\frac{\partial \eta}{\partial t} + H\left(\frac{\partial u}{\partial x} + \frac{\partial v}{\partial y}\right) = 0 \tag{4.34}$$

Given that $\omega \ll f$, $\frac{\partial}{\partial t} \ll 1$ and $\beta L/f_0 \ll 1$ we can approximate the mo-

mentum equations to a geostrophic flow

$$-f_0 v = -g\frac{\partial \eta}{\partial x} \tag{4.35}$$

$$f_0 u = -g\frac{\partial \eta}{\partial y} \tag{4.36}$$

and adding these geostrophic solutions to the shallow water equations

$$-f_0 v = -g\frac{\partial \eta}{\partial x} + \beta y \frac{g}{f_0}\frac{\partial \eta}{\partial x} + \frac{g}{f_0}\frac{\partial^2 \eta}{\partial y \partial t} \tag{4.37}$$

$$f_0 u = -g\frac{\partial \eta}{\partial y} + \beta y \frac{g}{f_0}\frac{\partial \eta}{\partial y} - \frac{g}{f_0}\frac{\partial^2 \eta}{\partial x \partial t} \tag{4.38}$$

The first part of the momentum equations is that of a geostrophic flow and the remaining is the small contribution from variations induced by the ageostrophic component. The last terms will be responsible for the propagation of Rossby waves.

Using continuity and (4.37)-(4.38) we arrive to

$$\frac{\partial \eta}{\partial t} - L_d^2 \partial_t \nabla^2 \eta - \beta L_d^2 \frac{\partial \eta}{\partial x} = 0 \tag{4.39}$$

which is a leading order approximation to the potential vorticity equation describing a quasi-geostrophic flow

$$\partial_t \left(\nabla^2 \eta - L_d^{-2} \eta \right) + \beta \frac{\partial \eta}{\partial x} = 0 \tag{4.40}$$

Now we can look for Fourier type solutions in the form $\eta = \eta_0 e^{i(kx+ly-\omega t)}$

$$\boxed{\omega = -\frac{\beta k}{(k^2+l^2)+L_d^{-2}}} \tag{4.41}$$

or alternatively

$$\omega = -\beta L_d^2 \frac{k}{1+L_d^2(k^2+l^2)} \tag{4.42}$$

Evidently, on the f-plane ($\beta = 0$) the solution reduces to a geostrophic flow and no wave is allowed to propagate. The meridional gradient in f is thus the restoring force for Rossby waves.

Two possible cases can be envisaged, setting $l = 0$.

First, that of short waves, where $L \leq L_d$ and therefore $kL_d \geq 1$, for L a typical scale of the wave length and k a typical scale of the wave number. In this case the dispersion relation reduces to

$$\omega = -\beta L_d^2 \frac{k}{L_d^2(k^2)} = -\frac{\beta}{k} = -\beta L \tag{4.43}$$

Given that we are on the β-plane approximation, $\beta y \ll f_0 \rightarrow \beta L \ll f_0 \rightarrow \omega \ll f_0$, confirming the subinterial period.

Second, waves could have very long wave length $L \geq L_d$ or $kL_d \leq 1$

$$\omega = -\beta L_d^2 k = -\beta \frac{L_d k^2}{k} \ll -\frac{\beta}{k} = -\beta L \tag{4.44}$$

and therefore $\omega \ll f_0$. The period of Rossby waves is always subinertial.

Phase and group speeds

Keeping $l = 0$ and using the following scaling

$$\omega = \hat{\omega}\beta L_d \tag{4.45}$$

$$\kappa = \frac{\hat{\kappa}}{L_d} \tag{4.46}$$

The dispersion relation takes the form

$$\hat{\omega}\beta L_d = -\beta L_d^2 \frac{\hat{\kappa}/L_d}{1 + L_d^2 \frac{\hat{\kappa}^2}{L_d^2}} \tag{4.47}$$

$$\hat{\omega} = -L_d \frac{\hat{\kappa}/L_d}{1 + \hat{\kappa}^2} = -\frac{\hat{\kappa}}{1 + \hat{\kappa}^2} \tag{4.48}$$

and for $|\hat{\kappa}| = -1$ the frequency takes the value $|\hat{\omega}| = -0.5$ (see Fig. 4.3).

The phase speed of Rossby waves is easily computed (with $l = 0$)

$$\boxed{c_p = \frac{\omega}{k} = \frac{-\beta}{k^2 + L_d^{-2}}} \tag{4.49}$$

it is always negative and larger for long waves .

For long Rossby waves, the phase velocity is approximated by

$$\boldsymbol{c_p} = \omega/\kappa = -\beta L_d^2 \tag{4.50}$$

which is strictly westward even if $l \neq 0$.

The phase speed is always negative but is the energy flux always directed westward? this does not seem possible.

The group velocity is obtained by differentiating the dispersion relation

$$\boldsymbol{c_g} = (\frac{\partial \omega}{\partial \kappa}, \frac{\partial \omega}{\partial l}) = \beta(\kappa^2 - l^2 - L_d^{-2}, 2\kappa l)/(\kappa^2 + l^2 + L_d^{-2})^2 \tag{4.51}$$

or, by setting $l = 0$

$$\boldsymbol{c_g} = \frac{\beta\kappa^2 - \beta L_d^{-2}}{(\kappa^2 + L_d^{-2})^2} \tag{4.52}$$

Set $k = 0$ and group and phase velocities are equal $c_p = c_g = -\beta L_d^2$ (see Fig. 4.3).

If $l \neq 0$ the dispersion relation takes the form of the dispersion diagram in Fig. 4.4. The group velocity, the gradient of the frequency in wavenumber space, is normal to the contours and inversely proportional to the spacing between contours. The hyperbola separating waves with eastward and

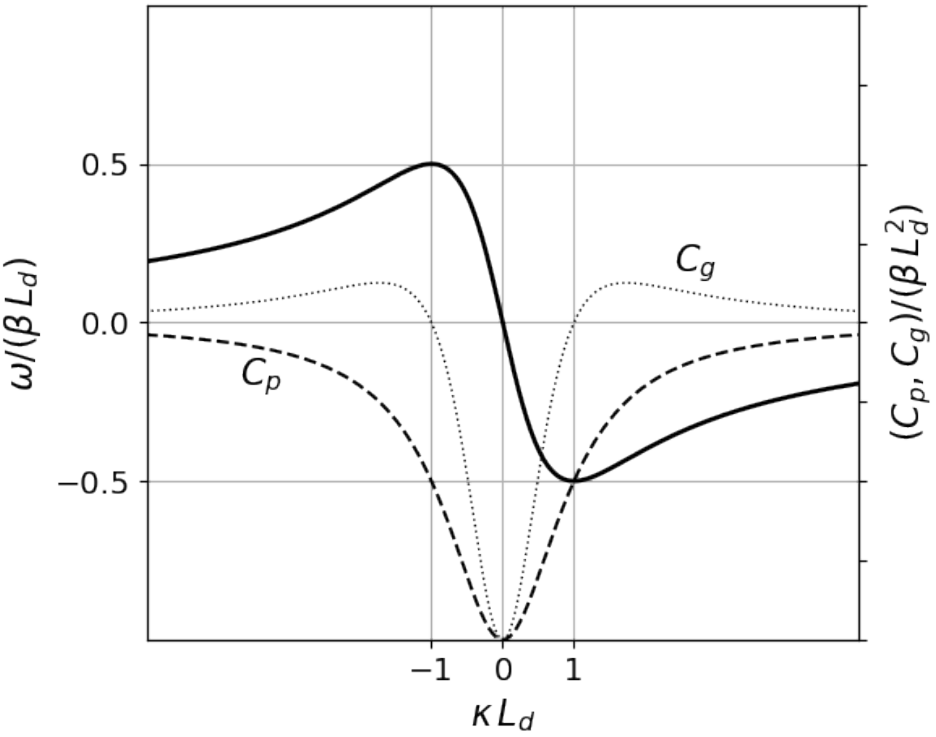

Figure 4.3: *Rossby wave dispersion relation, phase and group speeds.*

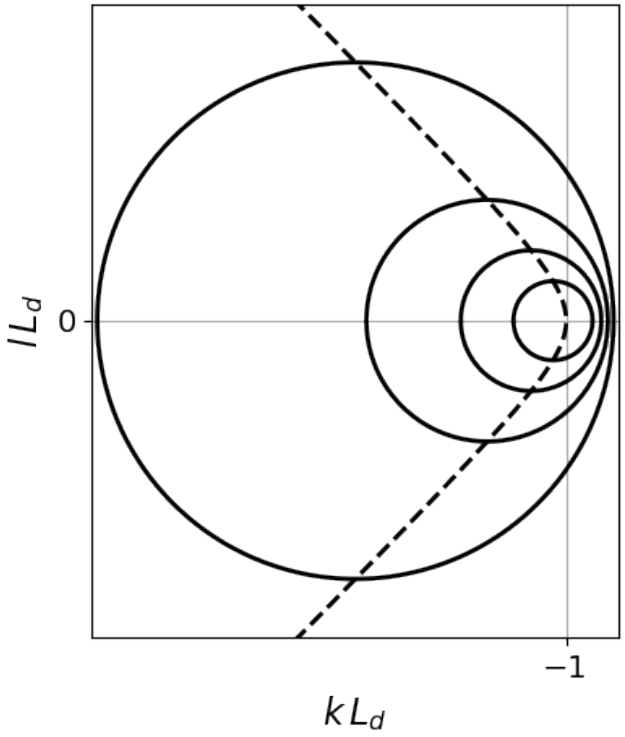

Figure 4.4: *Rossby wave dispersion diagram. Contours are of frequency in units of $\beta\, L_d$. The group velocity, the gradient of the frequency in wavenumber space, is normal to the contours and inversely proportional to the spacing between contours. The hyperbola separating waves with eastward and westward group velocity is shown by the dashed line and is $\kappa^2 = l^2 + L_d^{-2}$. Frequency contours reduce to a single point when $\omega = 0.5\beta L_d$ and $\kappa = L_d$.*

westward group velocity is shown by the dashed line and is $\kappa^2 = l^2 + L_d^{-2}$. Frequency contours reduce to a single point when $\omega = 0.5\beta L_d$ and $\kappa = L_d$.

4.3.1 Quasi-geostrophic Rossby waves

The discovery of Planetary waves by the solution of Laplace's equation as the second class waves dates back to the late nineteenth century by *Hough* (1897). Later C.G. Rossby pointed out the characteristic of these waves, hence they carry his name and are also called Rossby waves.

Since then, Rossby wave theory is well known (*Gill*, 1982; *Dickinson*, 1978; *Leblond and Mysak*, 1981) and is usually applied to an ocean at rest with uniform depth.

Rossby waves owe their existence to the meridional variation of the Coriolis force (the β effect) and therefore propagate following an east-west waveguide, as the conservation of potential vorticity is their restoring force.

These kinds of waves, whose frequencies are considerably lower than those of gravity waves and are subinertial ($\omega \ll f$), are also sometimes called quasigeostrophic waves, with a dynamic evolution depending on the departure from geostrophy.

The generation of these waves is still not completely understood but the main forcing is wind stress and buoyancy forcing, though the latter is thought to act in a minor way, and upwelling-downwelling on the eastern boundary (*Leblond and Mysak*, 1981; *Gill*, 1982).

In order to obtain and describe the Rossby wave solutions, we consider the linearised quasi-geostrophic (QG) potential vorticity equation (*Pedlosky*, 1987):

$$\partial_t q_i + J(\psi_i, q_i) = 0, \tag{4.53}$$

where $J(a,b) = a_x b_y - a_y b_x$ is the Jacobian and ψ the stream function. Introducing a plane wave solution of the type $\psi = \Psi e^{i(kx+ly-\sigma t)}$ into (4.53) we naturally obtain the dispersion relation for Rossby waves, showing their basic characteristics (*Leblond and Mysak*, 1981; *Gill*, 1982)

$$\omega = -\frac{\beta k}{(k^2+l^2)+L_d^{-2}},$$

where ω is the frequency, k and l are the horizontal wavenumber, β is the meridional variation of the Coriolis parameter and L_d the Rossby radius (C^2/f^2). It is clear that Rossby waves have westward phase velocities (of the order of a few cm/s) and that these are increasing toward the equator (where equatorial wave theory holds) with a maximum speed $c_x = \beta L_d^2$; the group velocities, C_g, in the case of long waves, are westward and the waves are nondispersive ($C_g = c_x$), while short waves propagate eastwards but with very slow speeds.

Another remarkable feature of the planetary wave dispersion relation is that not all frequencies exist, with a cutoff frequency at $\frac{1}{2}\beta L_d$.

Besides the horizontal problem, the vertical one is of great importance. Using a normal mode representation (*Leblond and Mysak*, 1981), separating the vertical and horizontal structure, we find an infinite set of solutions (or normal modes). The zeroth is the barotropic one, almost vertically independent and very rapid; the other solutions, or modes, are called baroclinic with decreasing phase speeds and increasing oscillation in the vertical. A first-mode baroclinic Rossby wave takes months to years to cross an ocean basin, depending on the latitude.

A 3-layer model

In the case of a 3-layer ocean, the potential vorticities are given by

$$\begin{aligned} q_1 &= \nabla\psi_1 + \beta y - F_{11}(\psi_1 - \psi_2) \\ q_2 &= \nabla\psi_2 + \beta y - F_{21}(\psi_2 - \psi_1) - F_{22}(\psi_2 - \psi_3) \\ q_3 &= \nabla\psi_3 + \beta y - F_{32}(\psi_3 - \psi_2), \end{aligned}$$

where $F_{m,n} = f_0^2/(H_m g'_n)$ and g'_i and H_i are the reduced gravities and layer depths respectively.

For this 3-layer system, substitution of a plane wave solution leads to a generalised eigenvalue problem of the form $\mathsf{A}\Psi = \omega\mathsf{B}\Psi$, or explicitly:

$$\begin{bmatrix} \beta_1 & 0 & 0 \\ 0 & \beta_2 & 0 \\ 0 & 0 & \beta_3 \end{bmatrix} \begin{bmatrix} \psi_1 \\ \psi_2 \\ \psi_3 \end{bmatrix} = \omega \begin{bmatrix} -G_1 & 1 & 0 \\ G_2 & -G_3 & 1 \\ 0 & 1 & -G_4 \end{bmatrix} \begin{bmatrix} \psi_1 \\ \psi_2 \\ \psi_3 \end{bmatrix},$$

where $\beta_1 = (k\beta)/F_{11}$, $\beta_2 = (k\beta)/F_{22}$, $\beta_3 = (k\beta)/F_{32}$ and $G_1 = (K^2 + F_{11})/F_{11}$, $G_2 = F_{21}/F_{22}$, $G_3 = (K^2 + F_{21} + F_{22})/F_{22}$, $G_4 = (K^2 + F_{32})/F_{32}$, where $K^2 = k^2 + l^2$.

The solution of the system is plotted in Fig.4.5 and it describes the basic properties of Rossby wave propagation. In fact, for the 3-layer system, the dispersion relation is found on the upper panel and both phase and group velocities on the bottom panel of Fig.4.5. We can distinguish the barotropic mode with increasing frequencies towards long wavelengths, very fast phase speeds and positive (eastward) group velocities. The baroclinc modes have smaller frequencies, their phase velocities are always westward but their group velocities turn from westward to eastward at the point of maximum frequency

$$kL_d = |1| \text{ and } \omega(\beta L_d)^{-1} = |0.5| \tag{4.54}$$

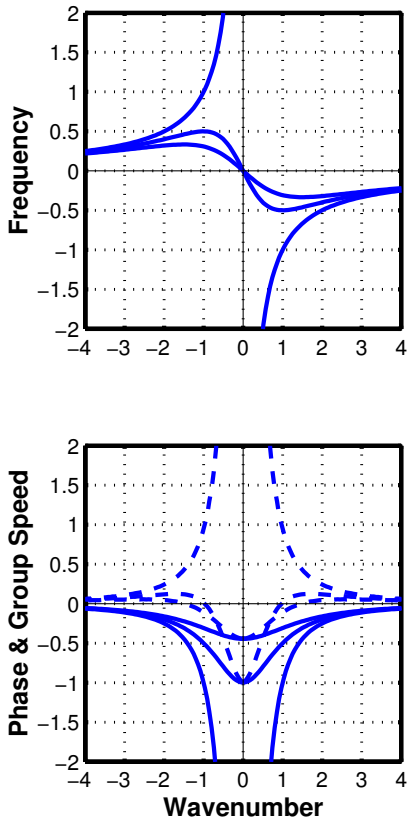

Figure 4.5: Upper panel: the dispersion relation for the barotropic and first two baroclinic modes of the 3-layer QG ocean. Shown are values of both positive and negative wavenumbers. The wavenumber is scaled by the deformation radius L_d and the frequency by βL_d; the meridional wavenumber l is set to zero. The first baroclinic mode frequency reaches a maximum at $\omega_{max} = \beta L_d/2$, i.e. $\omega_{max} = |0.5|$. Lower panel: phase (solid lines, $c_x = \omega/k$) and group (dashed lines, $Cg_x = \partial\omega/\partial k$) velocities of the barotropic and first two baroclinic modes, scaled by βL_d^2.

where the group velocity is zero. Therefore, long baroclinic waves direct their energy westward while short waves direct it eastward. This means that, in the limit of long wavelengths, the phase and group speeds are the same and the waves are nondispersive. On the other hand, for short waves phase and group speeds differ and the waves are dispersive. The maximum group and phase velocity ($C_x = Cg_x = -\beta L_d^2$) are attained for long waves, they are to the west and can be found on the axis origin of the dispersion relation.

The system could be extended to an N-layer or even to a continuously stratified ocean. In every case, the solutions obtained are one barotropic and N-1 baroclinic modes of decreasing phase speeds. This method of analysis is called the *normal modes method*, in which the ocean is decomposed into an infinite set of solutions (or modes): one barotropic (or external) and the remaining baroclinic (or internal).

4.3.2 Rossby waves in observations and models

Chelton and Schlax (1996) presented for the first time the results of these observations identifying clear Rossby waves signals (Fig.4.6) and common features like the increase of phase speed in the western basin, the effect of bottom topography, eastward propagating equatorially trapped Kelvin waves and pulses related to El Niño events.

As anticipated, the advent of satellite altimetry brought a powerful tool to describe Rossby waves in the real ocean. The TOPEX/POSEIDON (T/P) altimeter is able to detect long baroclinic planetary waves unambiguously over the entire world ocean (Fig. 4.7).

The T/P altimetry data reveal the sea surface height anomalies (SSHA) and to analyse this data time-longitude plots, known as Hovmöller diagrams, are used, which clearly show Rossby waves as diagonal alignments of crests and troughs moving westward. An example of this is given in Fig.4.7, where SSHA data from the Indian Ocean are plotted for the latitude 20^oS from 1993 till May 2005; in the left panel the row data are plotted while in the right panel the data have been filtered with a westward filter to better show Rossby wave propagation.

By this technique, Rossby waves are detected in all basins and altimetry has been used also in the Southern Ocean (*Hughes*, 1995) where two dynamical systems were found, a supercritical and a subcritical one with respect to Rossby waves, the first one being able to advect the waves east-

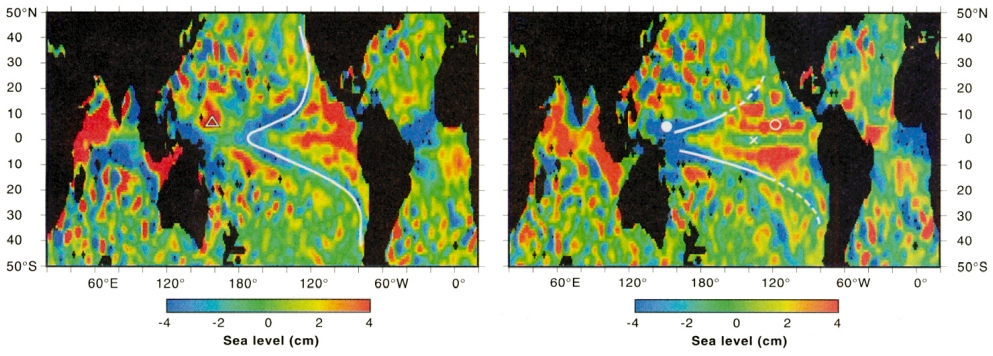

Fig. 4. Global maps of filtered sea level (*22*) on (**A**) 13 April 1993 (cycle 21) and 3.5 months later on (**B**) 31 July 1993 (cycle 32). White lines identify a westward-propagating, β-refracted Rossby wave trough. The time evolutions of the equatorial Kelvin wave trough (X), the Rossby wave crests (open triangle and open circle), and the Rossby wave trough (solid circle) can be traced from the times and locations of the matching symbols in Fig. 3. These two maps are frames from an animation of TOPEX/POSEIDON data that is available on the World Wide Web at http://topex-www.jpl.nasa.gov/contrib/chelton/rossby/.

Figure 4.6: Sea surface height anomalies showing the propagation of planetary waves in the Pacific Ocean. Also clear is the β-effect inducing larger phase speeds towards the equator [from *Chelton and Schlax* (1996)].

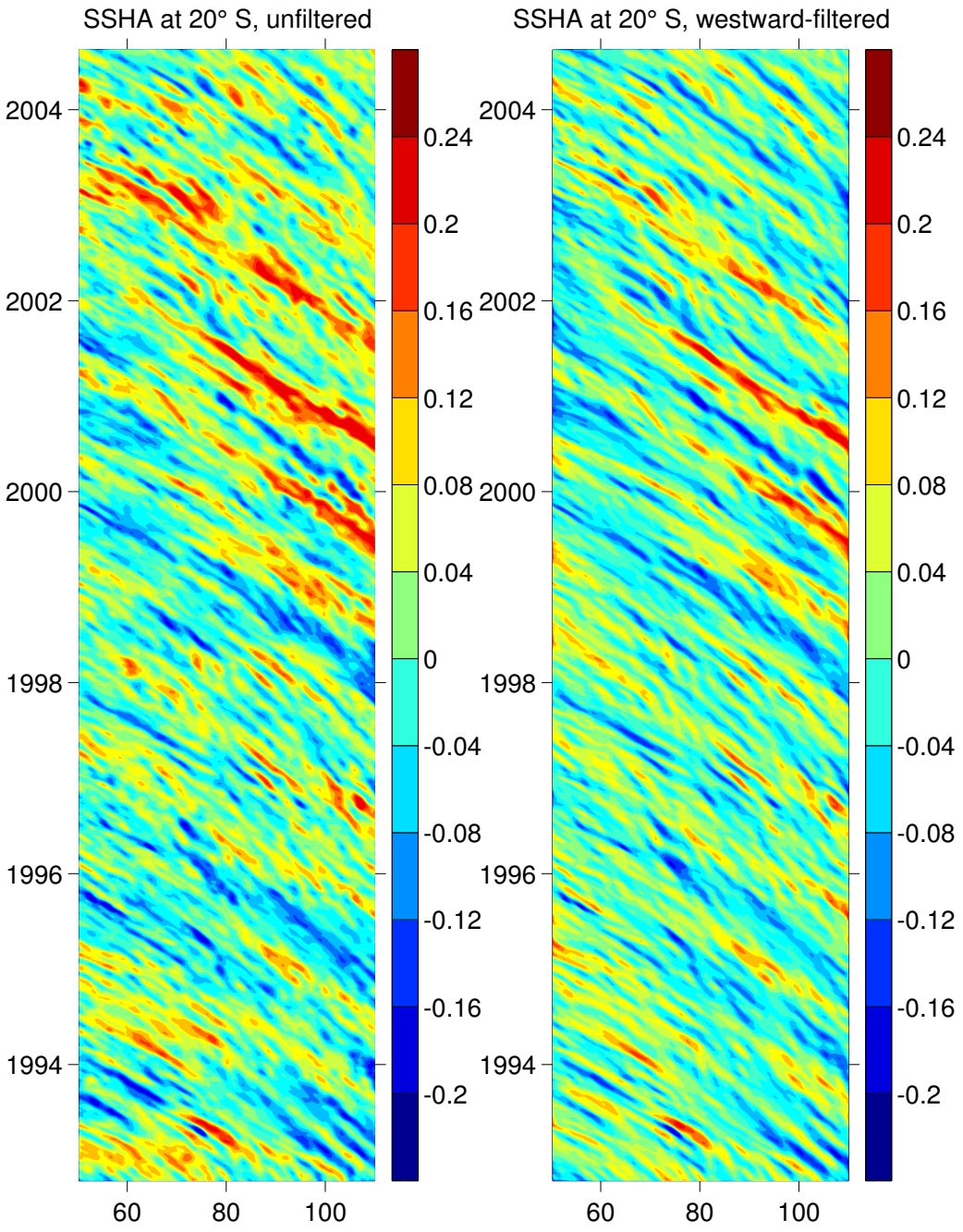

Figure 4.7: Time-longitude plot of the sea surface height anomalies (in meters) in the Indian Ocean at 20^oS. On the left panels, the original altimeter data. On the right panel, the corresponding westward-filtered signature. There is a clear evidence of crests and troughs propagating westward with a biannual period (Courtesy of P. Cipollini).

ward.

Rossby waves are also detected by other sensors like the Along-track Scanning Radiometer (ATSR) in sea surface temperature (SST) and, recently, SeaWiFS in ocean colour.

As an example, *Hill et al.* (2000) used a SST record to compute Rossby wave phase speeds finding good agreement with *Killworth et al.* (1997). They were also able to detect topographic effects such as those predicted by *Killworth and Blundell* (1999).

One of the latest applications has been using ocean colour. *Cipollini et al.* (2001) found for the first time Rossby waves in SeaWiFS datasets, although they are neither very clear nor ubiquitous. A preliminary explanation for this detectability was in term of the vertical displacements of the thermocline associated with the Rossby wave and subsequently changes in the nutrient upwelling.

Computing Rossby wave phase speeds

In order to compute the gravity wave phase speeds and Rossby radii of deformation we need to solve the generalized eigenvalue problem of Sturm-Liouville form:

$$\frac{d^2\phi}{dz^2} + \frac{N^2(z)}{C^2}\phi = 0 \tag{4.55}$$

subject to the following boundary conditions

$$\phi = 0 \qquad at \quad z = 0, -H \tag{4.56}$$

where H is the local mean water depth and N^2 is the Brunt-Väisälä frequency, computed from the potential density method as outlined in *Chelton et al.* (1998). Solution of the system (4.55)-(4.56) leads to an infinite set of eigenvalues C_m^{-2}, the baroclinic gravity wave phase speeds, and corresponding eigenfunctions ϕ_m.

However, *Chelton et al.* (1998) showed that a WKB approximation of the gravity wave speed is generally in good agreement with the solution given by the system (4.55)-(4.56), and this is:

$$C_m \approx C_m^{WKB} = (m\pi)^{-1} \int_{-H}^{0} N(z)\mathrm{d}z, \quad m \geq 1. \tag{4.57}$$

Then, within the extratropical regions, the Rossby radii of deformation are simply found by applying

$$L_d^m = \frac{C_m}{|f(\theta)|}. \tag{4.58}$$

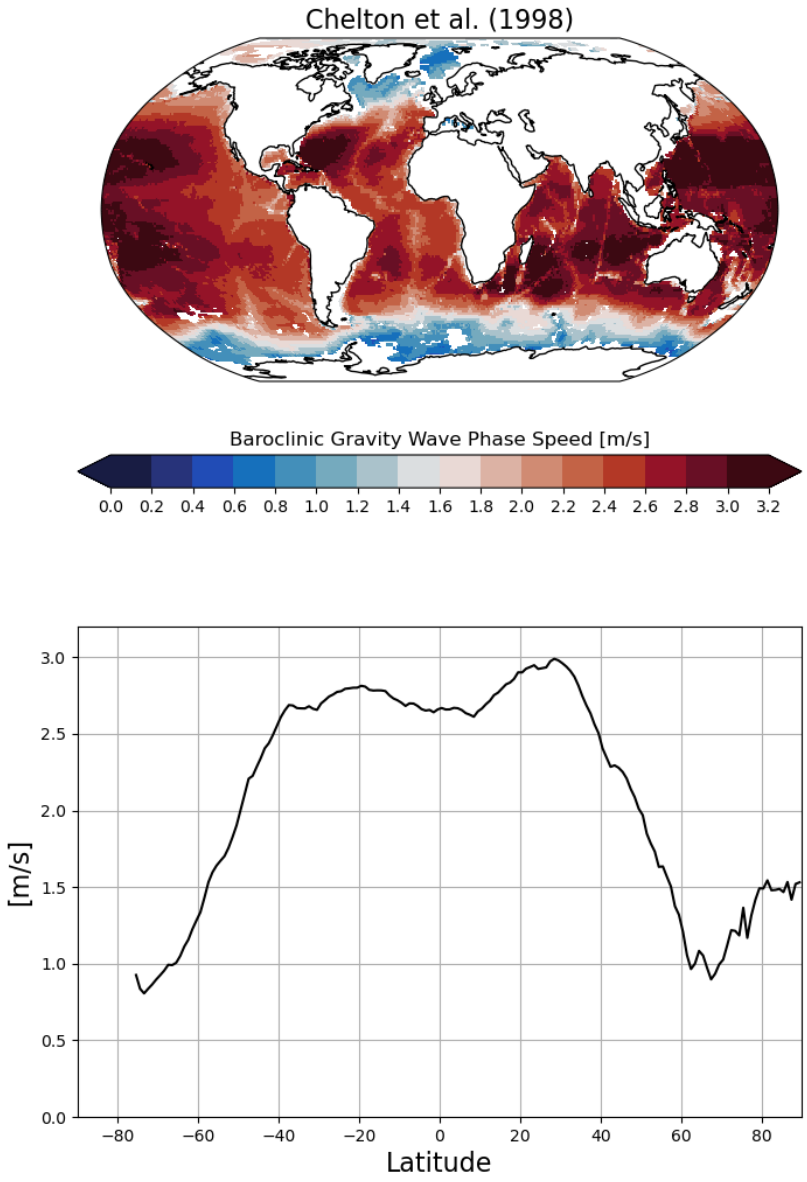

Figure 4.8: *A global contour map of the baroclinic gravity wave phase speed [from Chelton et al., 1998] and its zonal mean.*

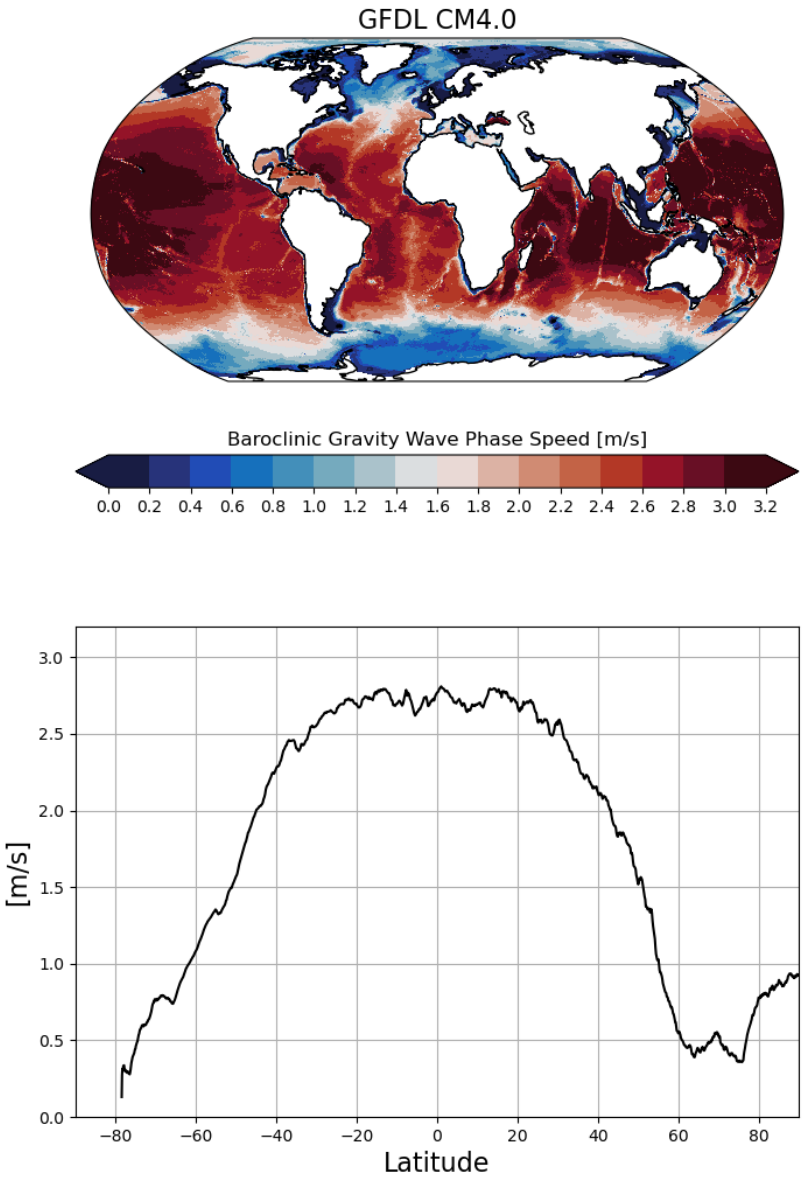

Figure 4.9: *As in Fig.4.8 but from the GFDL-CM4.0 model under historical conditions for years 2010-2014.*

We will be focusing on extratropical regions only ($|\theta| \geq 10^\circ$), leaving the equatorial wave dynamics response aside.

Now, we can compute the unperturbed long Rossby wave speeds $c_m = -\beta C_m^2 / f^2$.

Since model data provide potential density ρ_θ, we can compute the stratification directly from the potential density method of the non-equispaced vertical levels k:

$$N^2(z) = -g/\rho_0 \Big[\rho_\theta(z) - \rho_\theta(z+1)/(\delta k(z) - \delta k(z+1))\Big] \tag{4.59}$$

The gravity wave speed can be obtained from two different method. First, as a good approximation, we can infer it from the WKB method as suggested in *Chelton et al.* (1998):

$$C_m = (m\pi)^{-1} \int_{-H}^{0} N(z)\mathrm{d}z, \quad m \geq 1. \tag{4.60}$$

After obtaining N^2 and C_m, the Rossby radii of deformation are readily computed as

$$L_d^m = \frac{C_m}{|f(\theta)|}, \quad |\theta| \geq 5^\circ \tag{4.61}$$

$$L_d^m = \frac{C_m}{2|\beta(\theta)|}, \quad |\theta| \leq 5^\circ. \tag{4.62}$$

or, for the extratropical band: $L_d^m = (|f|m\pi)^{-1} \int_{-H}^{0} N(z)\mathrm{d}z$

For the linear, long and extratropical waves, we can simply compute the Rossby wave phase speed as

$$c_m = -\beta (L_d^m)^2 \tag{4.63}$$

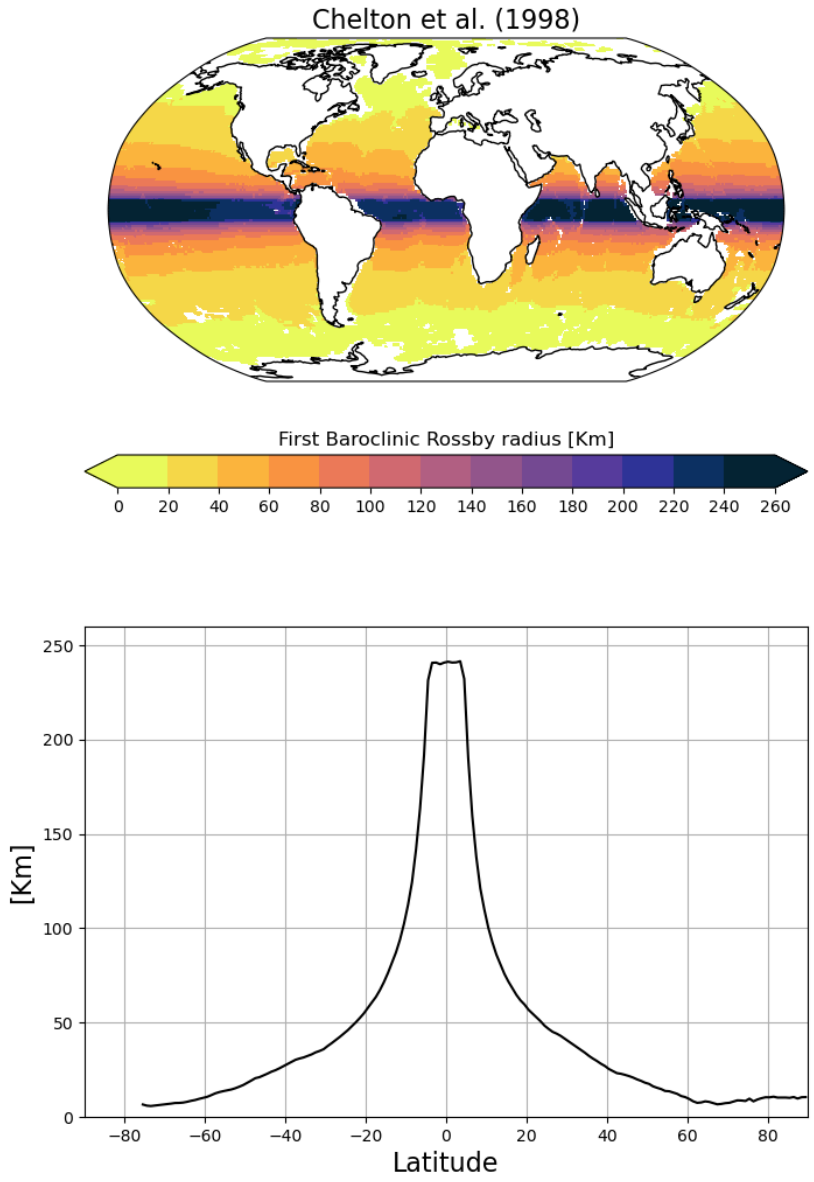

Figure 4.10: *A global contour map of the baroclinic Rossby radius of deformation and its zonal mean. [data from Chelton et al., 1998]*

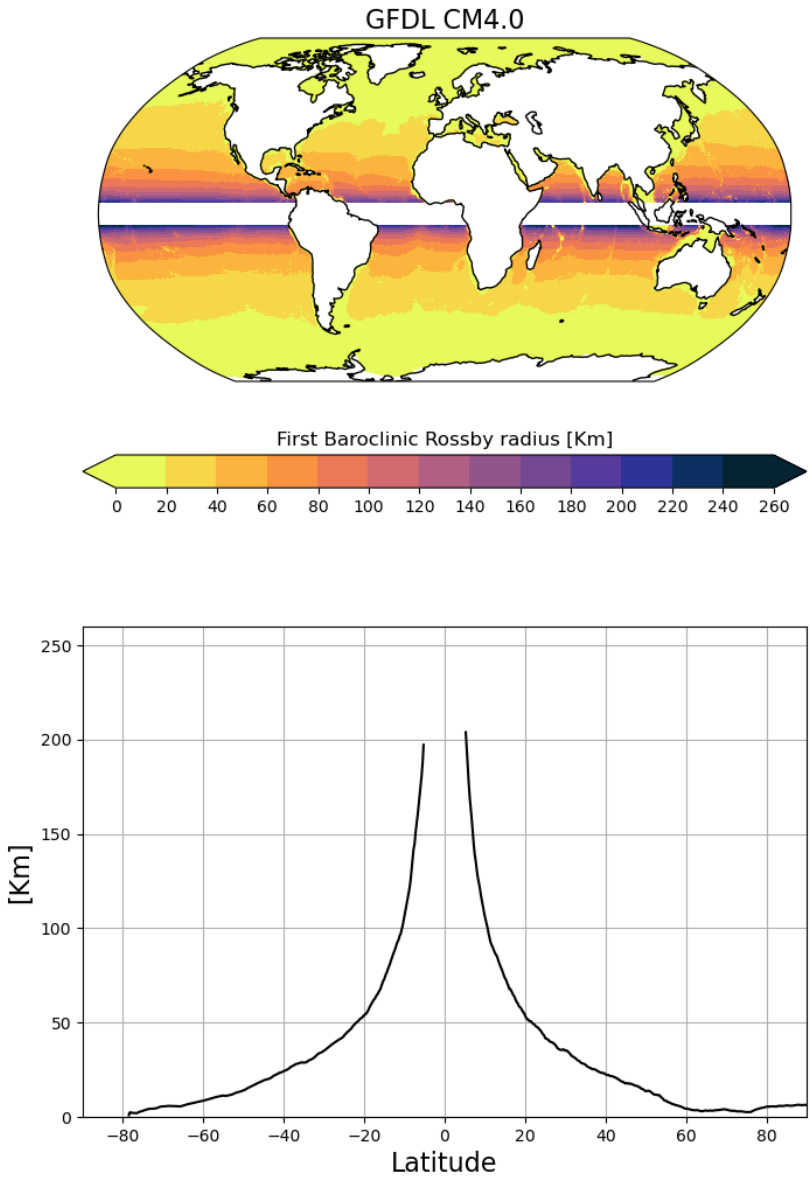

Figure 4.11: *As in Fig.4.10 but from the GFDL-CM4.0 model under historical conditions for years 2010-2014.*

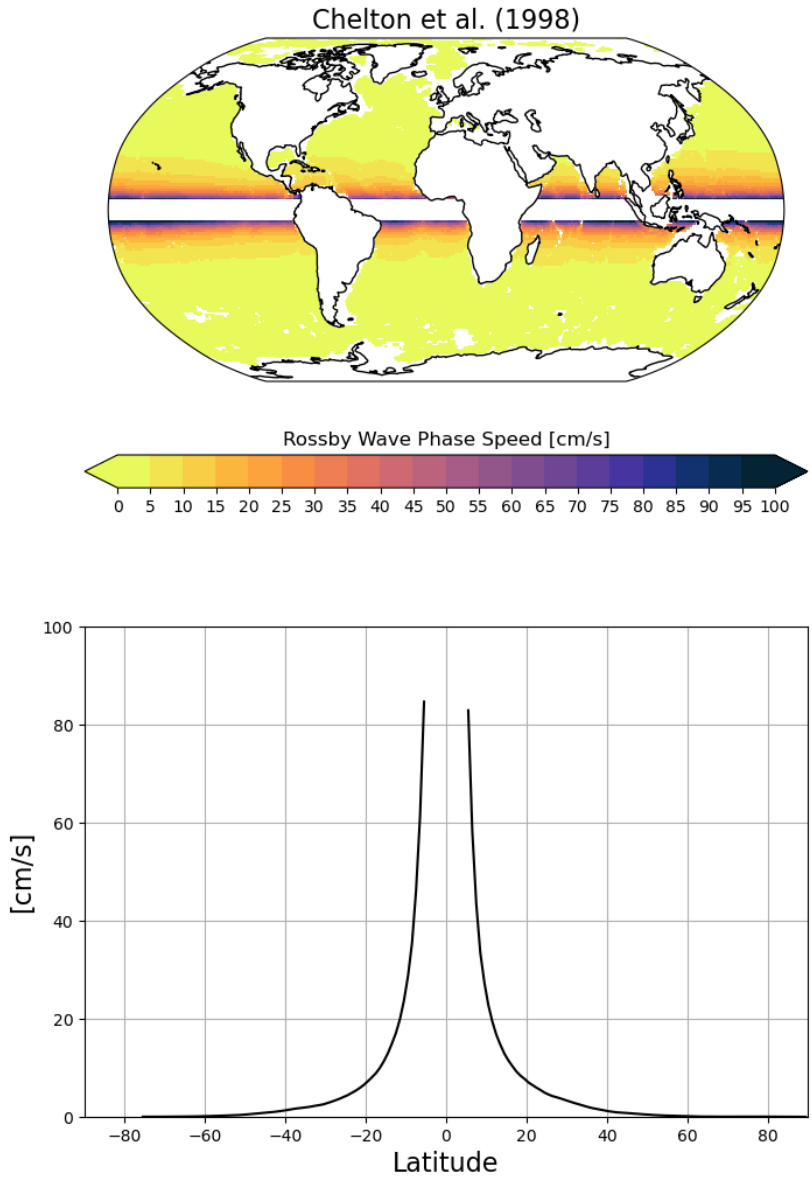

Figure 4.12: *A global contour map of the baroclinic Rossby wave phase speed and its zonal mean. [data from Chelton et al., 1998]*

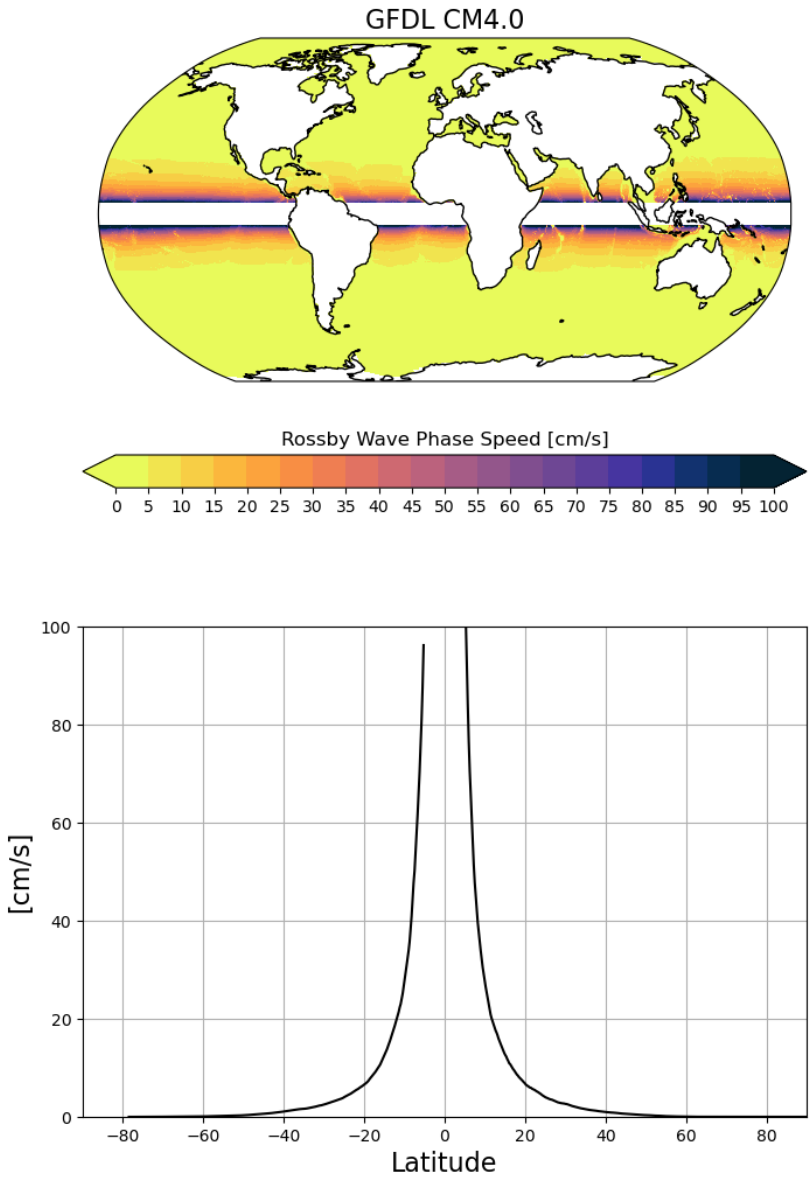

Figure 4.13: *As in Fig.4.12 but from the GFDL-CM4.0 model under historical conditions for years 2010-2014.*

Kelvin and Rossby waves in the general oceanic adjustment

The importance of Rossby waves in the spinup of the ocean and in the adjustment of the ocean interior was also recently shown by *Johnson and Marshall* (2002). They proposed a theory for surface Atlantic response to thermohaline variability; in their work they study the reaction of the ocean to a perturbation of the rate of deep water formation at high latitudes. These changes initiate Kelvin waves which propagate along the western boundary, in a similar response of that demonstrated by *Kawase* (1987), and then cross the basin as equatorial Kelvin waves until they reach the eastern boundary where they propagate northwards and southwards. The final part of the response is the radiation of Rossby waves from the eastern boundary, communicating the thermocline displacement to the ocean interior which is clearly illustrated with a series of snapshots (Fig. 4.14).

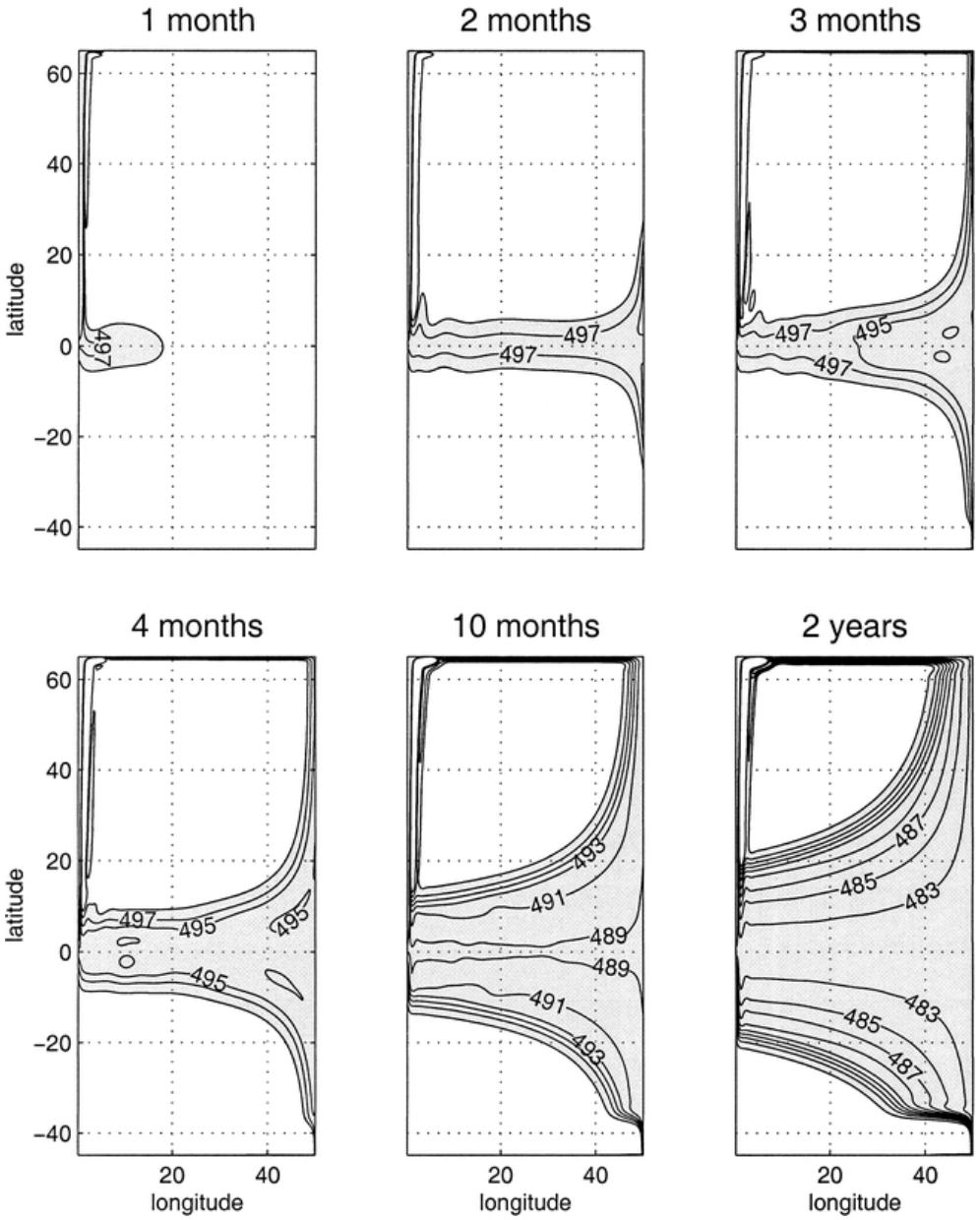

Figure 4.14: *Surface layer thickness after a thermohaline overturning of 10 Sv is switched on at time t = 0 in the northwest corner of an ocean initially at rest. There is no wind forcing, and the surface layer is initially 500 m deep. The contour interval is 2 m, and thicknesses less than 499 m are shaded. Note that the thickness anomaly on the western boundary is much greater than that in the interior. [from Johnson and Marshall, JPO2022]*

What will happen in the future?

Saenko (2006) recently showed that, within the IPCC models, there is clear evidence of an increase of the first baroclinic Rossby radius with increasing oceanic stratification in the warmer climate. The changes range from 15 to 20% depending on the model and latitude. This would imply a greater length scale for mesoscale eddies and modified characteristics for oceanic Rossby waves, whose speed is proportional to the squared baroclinic Rossby radius of deformation. Also, the adjustment time scale in the ocean would decrease as well as in any ocean-atmosphere climate variability process where Rossby waves set the dominant period. Equally important, if not more in certain basins, is the change in the background baroclinic mean flow and its subsequent effect on the propagation of Rossby waves. This effect was not considered in *Saenko* (2006).

Modifications to the background stratification and mean flows are observed between pre-industrial and climate-change runs in the GFDL CM4 model (Fig.4.15 and Fig.4.16).

The effects of an increased stratification on the Rossby radius of deformation and gravity wave speed have been the subject of recent studies (*Saenko*, 2006). However, the question of the quantification of these effects on the Rossby wave activity, as well as the changes induced by a modified background mean flow, is still unanswered.

We expect to show considerable alterations to the Rossby wave phase speeds at different latitudes, leading to important changes in the ocean adjustment time-scale and coupled ocean-atmosphere interactions where Rossby waves set the clock (Fig.4.19 and Fig.4.20).

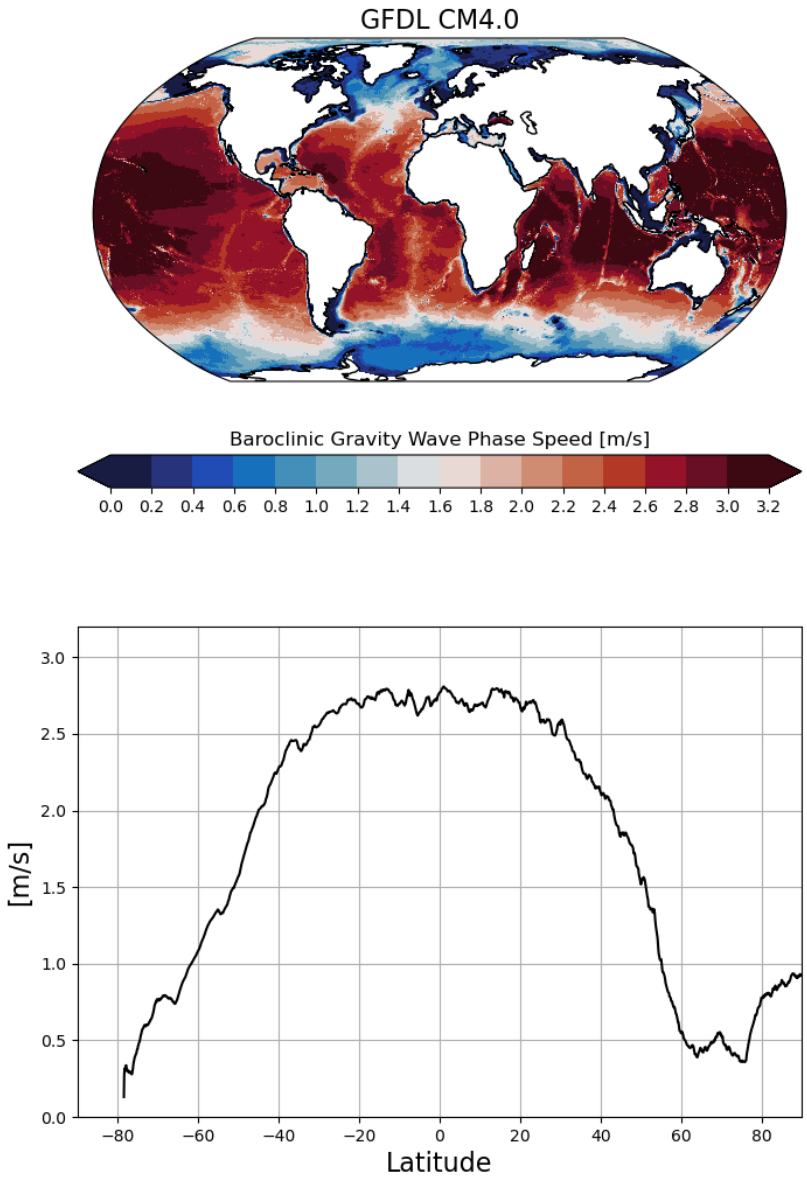

Figure 4.15: *The baroclinic gravity wave phase speed computed from the GFDL-CM4.0 model under historical conditions for years 2010-2014.*

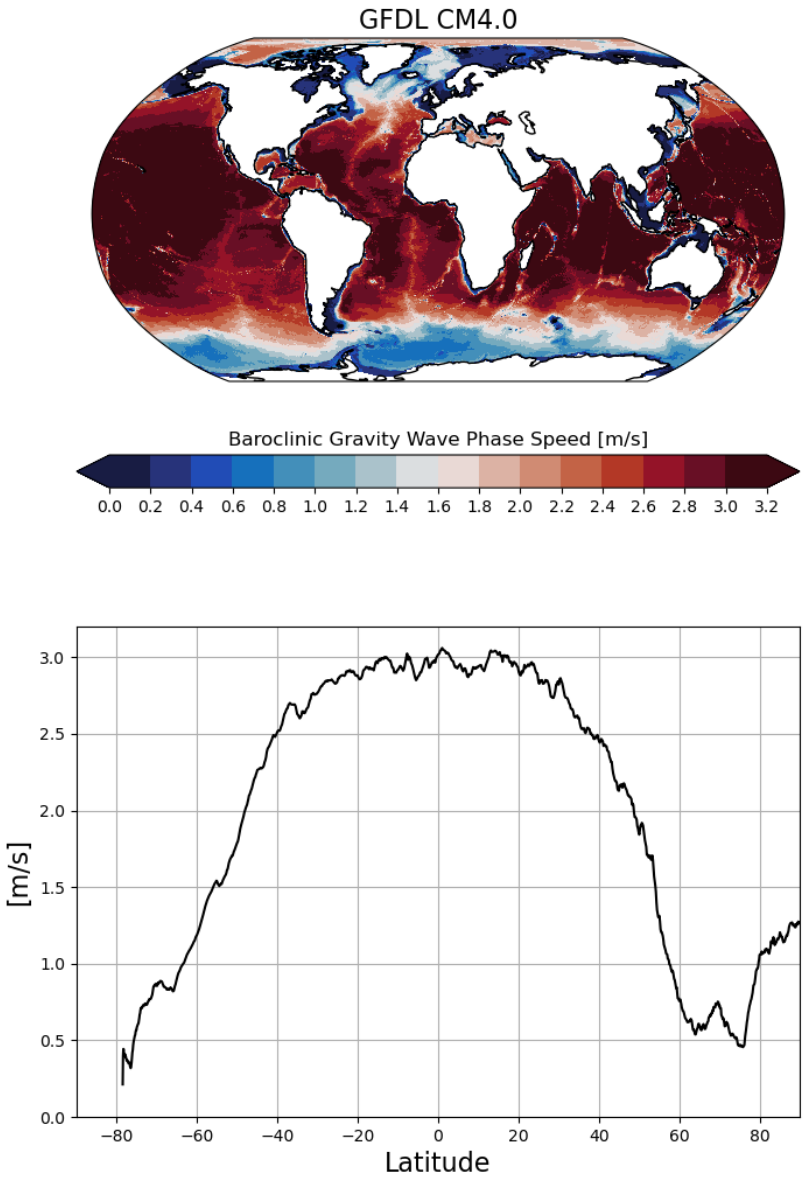

Figure 4.16: *The baroclinic gravity wave phase speed computed from the GFDL-CM4.0 model for the future scenario SSP585.*

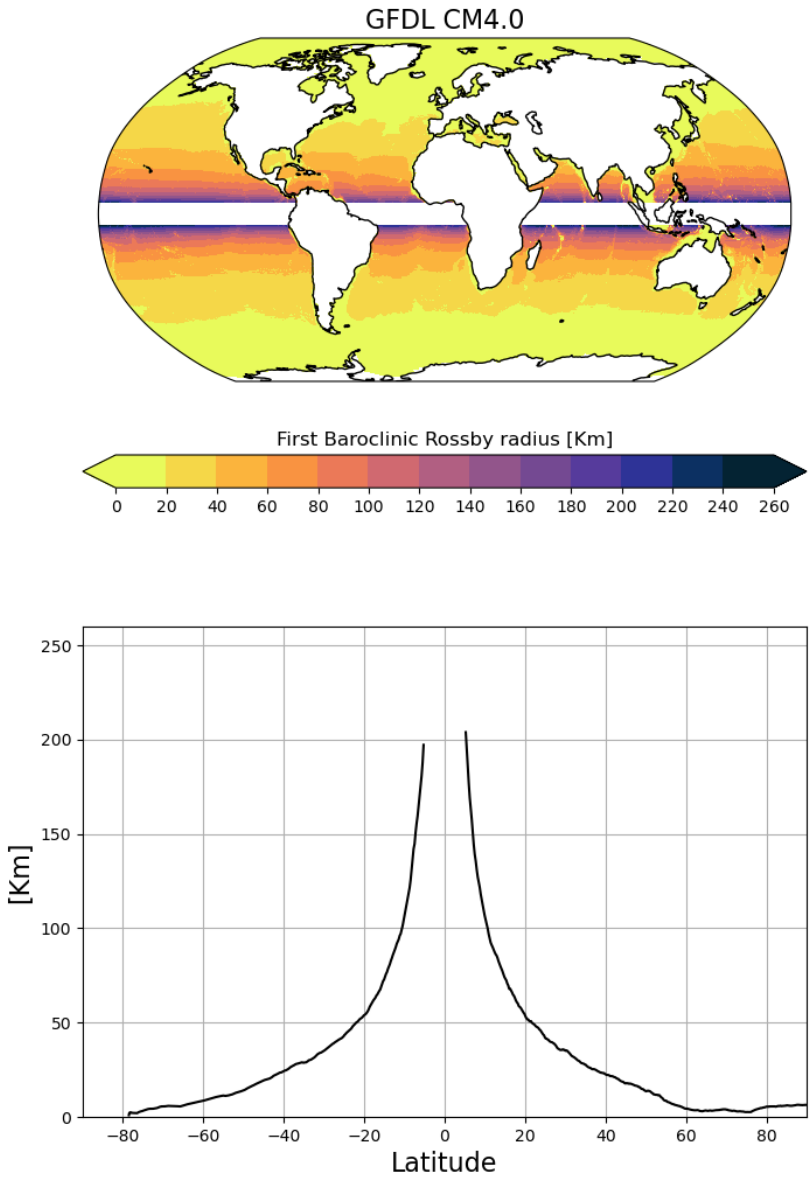

Figure 4.17: *The Rossby radius computed from the GFDL-CM4.0 model under historical conditions for years 2010-2014.*

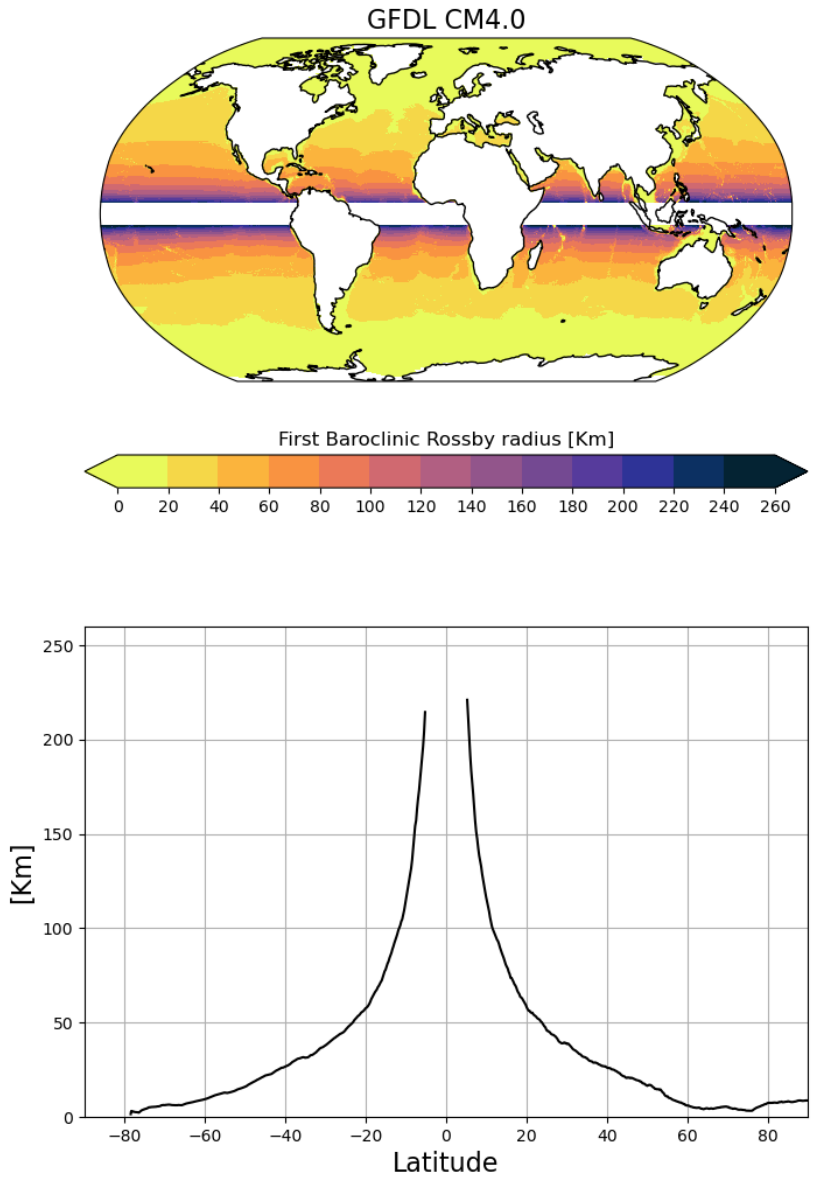

Figure 4.18: *The Rossby radius computed from the GFDL-CM4.0 model for the future scenario SSP585.*

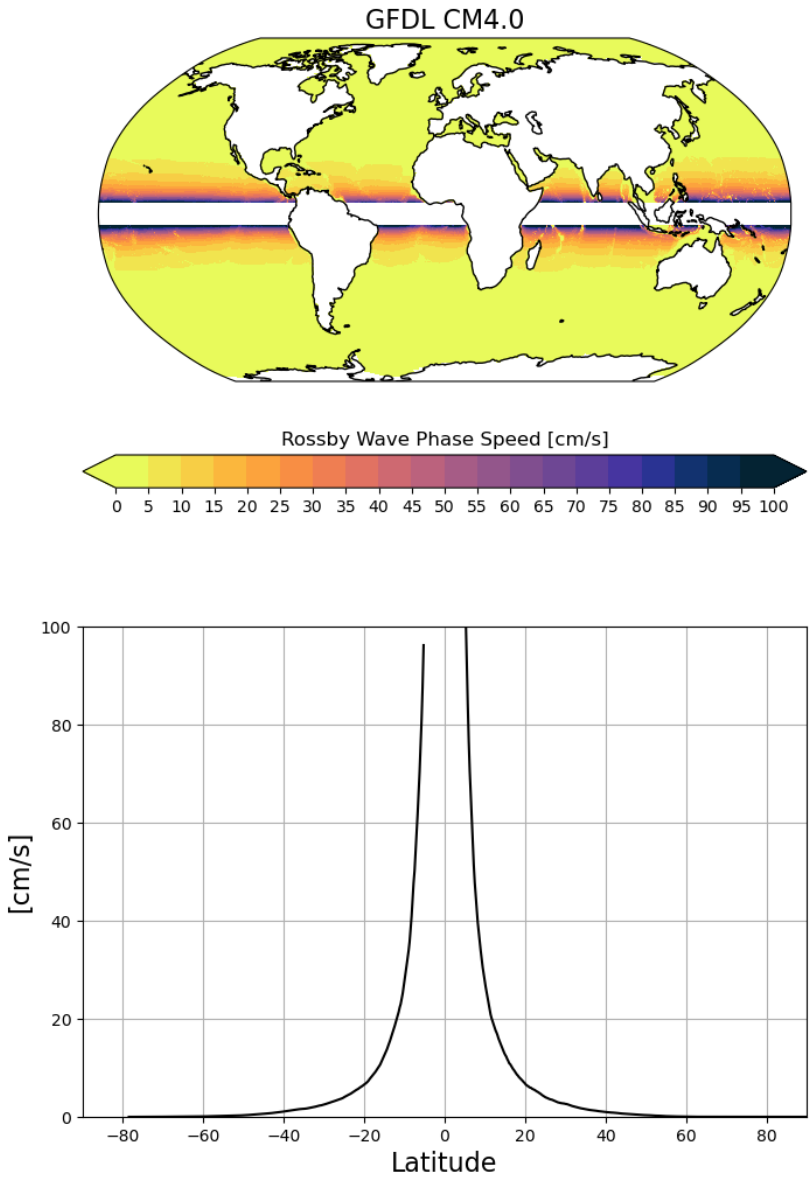

Figure 4.19: *The baroclinic Rossby wave phase speed computed from the GFDL-CM4.0 model under historical conditions for years 2010-2014.*

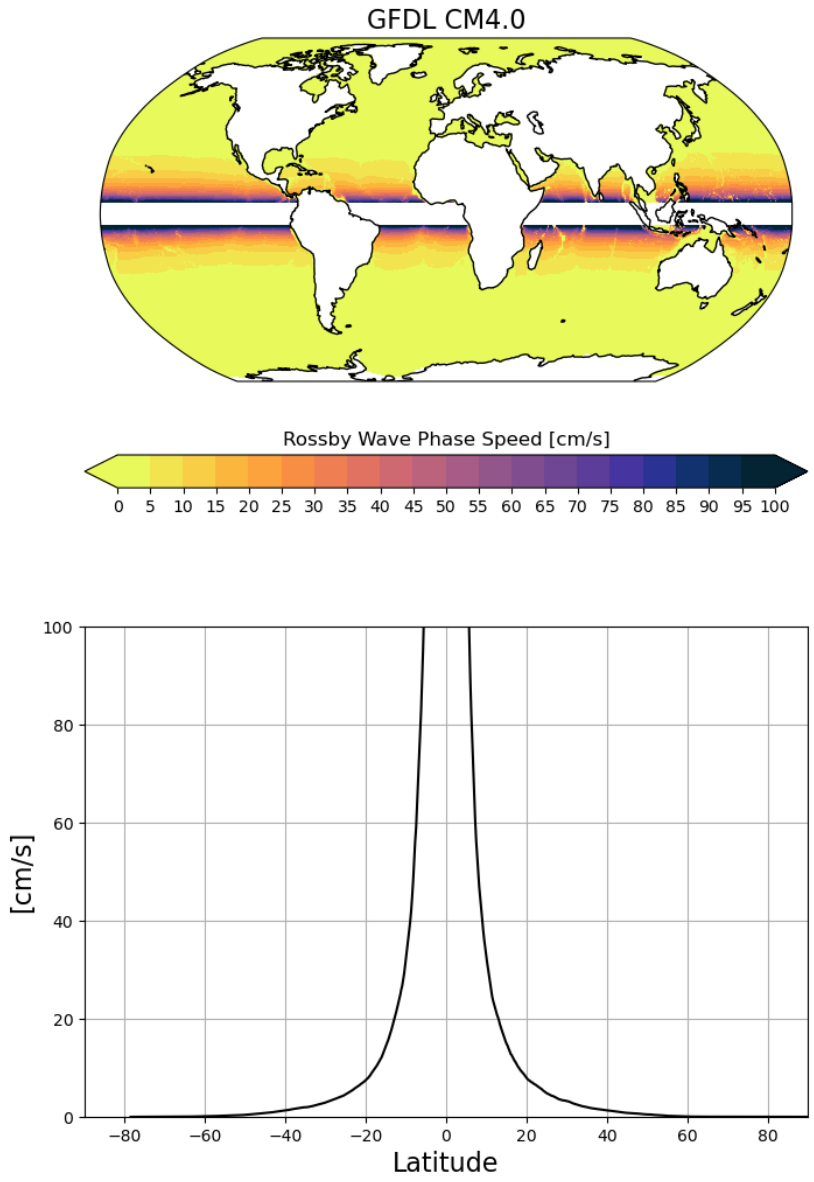

Figure 4.20: *The baroclinic Rossby wave phase speed computed from the GFDL-CM4.0 model for the future scenario SSP585.*

Bibliography

Anderson, D. L. T., and A. E. Gill, Spin-up of a stratified ocean, with application to upwelling, *Deep-Sea Res.*, *22*, 583–596, 1975.

Anderson, D. L. T., and A. E. Gill, Beta-dispersion of inertial waves, *J. Geophys. Res.*, *84*, 1836–1842, 1979.

Cessi, P., and P. Otheguy, Oceanic teleconnections: Remote response to decadal wind forcing, *J. Phys. Oceanogr.*, *33*, 1604–1617, 2003.

Chelton, D. B., and M. G. Schlax, Global observations of oceanic rossby waves, *Science*, ***272***, 234–238, 1996.

Chelton, D. B., R. A. deSzoeke, M. G. Schlax, K. E. Naggar, and N. Siwertz, Geographical variability of the first baroclinic rossby radius of deformation, *J. Phys. Oceanogr.*, ***28***, 433–460, 1998.

Cipollini, P., D. Cromwell, P. G. Challenor, and S. Raffaglio, Rossby waves detected in global ocean colour data, *Geophys. Res. Lett.*, ***28***, 323–326, 2001.

Dewar, W., On ocean dynamics in midlatitude climate, *J. Climate*, ***14***, 4380–4397, 2001.

Dickinson, R. E., Rossby waves-long period oscillations of oceans and atmosphere, *Annu. Rev. Fluid Mech.*, ***10***, 159–195, 1978.

Galanti, E., and E. Tziperman, A midlatitude-enso teleconnection mechanism via baroclinically unstable long rossby waves, *J. Phys. Oceanogr.*, ***33***, 1877–1888, 2003.

Gill, A. E., *Atmosphere-Ocean Dynamics*, *International Geophysics Series*, vol. **30**, 662 pp., Academic Press, 1982.

Hill, K. L., I. Robinson, and P. Cipollini, Propagation characteristics of extratropical planetary waves observed in the atsr global sea surface temperature record, *J. Geophys. Res.*, ***105***, 21,927–21,945, 2000.

Hough, S., On the application of harmonic analysis to the dynamical theory of the tides, part i, on laplace's oscillations of the first species, and on the dynamics of ocean currents, *Phil. Trans. Roy. Soc. Lond.*, *189*, 201–257, 1897.

Hughes, C. W., Rossby waves in the southern ocean: A comparison of topex/poseidon altimetry with model predictions, *J. Geophys. Res.*, ***100***, 15,933–15,950, 1995.

Johnson, H. L., and P. Marshall, A theory for the surface atlantic response to thermohaline variability, *J. Phys. Oceanogr.*, ***32***, 1121–1132, 2002.

Kalnay, E., M. Kanamitsu, R. Kistler, W. Collins, D. Deaven, L. Gandin, M. Iredell, S. Saha, G. White, J. Woollen, Y. Zhu, M. Chelliah, W. Ebisuzaki, W. Higgins, J. Janowiak, K. Mo, C. Ropelewski, J. Wang, A. Leetmaa, R. Reynolds, R. Jenne, and D. Joseph, The NCEP/NCAR 40-year reanalysis project, *Bull. Amer. Meteor. Soc.*, *77*, 437–471, 1996.

Kawase, M., Establishment of deep ocean circulation driven by deep-water production, *J. Phys. Oceanogr.*, ***17***, 2294–2317, 1987.

Killworth, P. D., and J. R. Blundell, The effect of bottom topography on the speed of long extratropical planetary waves, *J. Phys. Oceanogr.*, ***29***, 2689–2710, 1999.

Killworth, P. D., D. B. Chelton, and R. A. de Szoeke, The speed of observed and theoretical long extratropical planetary waves, *J. Phys. Oceanogr.*, ***27***, 1946–1966, 1997.

Kuhlbrodt, T., A. Griesel, M. Montoya, A. Levermann, A. Hofmann, and S. Rahmstorf, On the driving processes of the atlantic meridional overturning circulation, *Reviews of Geophysics*, *45*, RG2001.10.1029/2004RG000,166, 2007.

Leblond, P. H., and L. A. Mysak, *Waves in the Ocean*, 1st ed., 602 pp., Elsevier Oceanography Series, 1981.

Olbers, D., J. Willebrand, and C. Eden, *Ocean Dynamics*, Springer-Verlag, 704 pp, 2012.

Pedlosky, J., *Geophysical Fluid Dynamics*, 2nd ed., Springer-Verlag, 724 pp, 1987.

Pierce, D., T. P. Barnett, N. Schneider, R. Saravanan, D. Dommenget, and M. Latif, The role of ocean dynamics in producing decadal climate variability in the north pacific, *Climate Dyn.*, *18*, 51–70, 2001.

Saenko, O. A., Influence of global warming on baroclinic rossby radius in the ocean: a model intercomparison, *J. Climate*, *19*, 1354–1360, 2006.

Talley, L., Simple coupled midlatitude climate models, *J. Phys. Oceanogr.*, ***29***, 2016–2037, 1999.

Talley, L., G. L. Pickard, W. J. Emery, and J. H. Swift, *Descriptive Physical Oceanography*, Academic Press, 560 pp, 2011.

Vallis, G. K., *Atmospheric and Oceanic Fluid Dynamics*, Cambridge Univ. Press, 745 pp, 2006.

Vallis, G. K., *Essentials of Atmospheric and Oceanic Dynamics*, Cambridge Univ. Press, 356 pp, 2019.